



# 1 Tectonostratigraphic evolution of the Slyne Basin

2 Conor M. O'Sullivan <sup>1,2,4</sup>, Conrad J. Childs <sup>1,2</sup>, Muhammad M. Saqab <sup>1,2,5</sup>, John J. Walsh <sup>1</sup>,  
3 <sup>2</sup>, Patrick M. Shannon <sup>1,3</sup>

4 <sup>1</sup> Irish Centre for Research in Applied Geoscience (iCRAG), O'Brien Centre for Science (East), University College  
5 Dublin, Belfield, Dublin 4, Ireland

6 <sup>2</sup> Fault Analysis Group, School of Earth Sciences, University College Dublin, Belfield, Dublin 4, Ireland

7 <sup>3</sup> School of Earth Sciences, University College Dublin, Belfield, Dublin 4, Ireland

8 <sup>4</sup> Present address: Petroleum Experts, Petex House, 10 Logie Mill, Edinburgh, EH7 4HG, United Kingdom

9 <sup>5</sup> Present address: Norwegian Geotechnical Institute, 40 St. Georges Terrace, Perth, WA 6000, Australia

10 Corresponding author email: cmnosullivan@gmail.com

## 11 1. Abstract

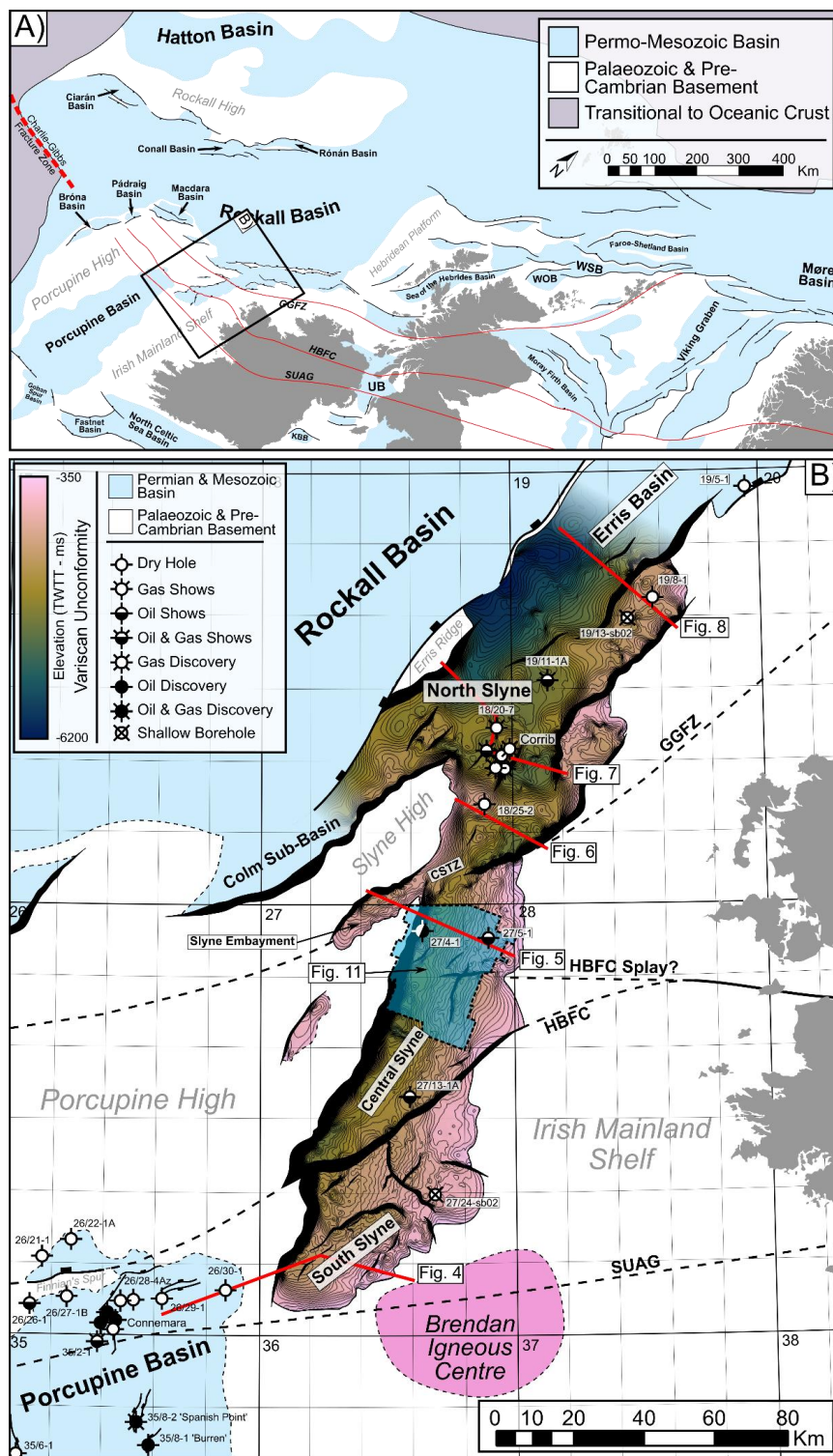
12 The Slyne Basin, located offshore NW Ireland, is a narrow and elongate basin composed of a  
13 series of interconnected grabens and half-grabens, separated by transfer zones coincident  
14 with deep Caledonian-aged crustal structures. The basin is the product of a complex,  
15 polyphase structural evolution stretching from the Permian to the Miocene. Relatively low-  
16 strain episodic rifting occurred in the Late Permian and the latest Triassic to Middle Jurassic,  
17 with the main phase of rifting occurring in the Late Jurassic. These extensional events were  
18 punctuated by periods of tectonic quiescence during the Early Triassic, and regional uplift and  
19 erosion during the late Middle Jurassic. Late Jurassic strain was primarily accommodated by  
20 several kilometres of slip on the basin-bounding faults, which formed through the breaching of  
21 relay ramps between left-stepping fault segments developed during earlier Permian and Early-  
22 Mid Jurassic rift phases. Following the cessation of rifting at the end of the Jurassic, the area  
23 experienced kilometre-scale uplift and erosion during the Early Cretaceous and second, less-  
24 severe phase of denudation during the Palaeocene. These post-rift events formed a distinct  
25 regional post-rift unconformity and resulted in a reduced post-rift sedimentary section. The  
26 structural evolution of the Slyne Basin is influenced by pre-existing Caledonian structures at a  
27 high angle to the basinal trend. The basin illustrates a rarely documented style of fault  
28 reactivation in which basin-bounding faults are oblique to the earlier structural trend, but the  
29 initial fault segments are parallel to this trend. The result is a reversal of the sense of stepping  
30 of the initial fault segments generally associated with basement control on basin-bounding  
31 faults.

32



## 33 2. Introduction

34 The north-western European Atlantic margin is made up of a framework of basins which are  
35 the product of a polyphase geological evolution stretching from Variscan orogenic collapse to  
36 the formation of oceanic crust during the opening of the North Atlantic Ocean (Fig. 1A). The  
37 evolution of these basins is influenced by a variety of factors, including pre-existing faults and  
38 lineaments, typically inherited from the Caledonian or Variscan orogenies, and the presence  
39 of salt within the sedimentary basin-fill, acting as layers of mechanical detachment. Pre-  
40 existing structures have been observed both reactivating during later rift events if oriented  
41 optimally (e.g. Stein, 1988; Schumacher, 2002; Wilson et al., 2010; Bird et al., 2014; Fazlikhani  
42 et al., 2017; Osagiede et al., 2020) or acting as barriers to fault growth and segmenting rift  
43 systems if they are oblique to the extension direction (e.g. Morley et al., 2004; Pereira et al.,  
44 2011; Philips et al., 2018).





46 **Figure 1: A)** Simplified structural map of the NW European Atlantic margin showing the study  
47 area in relation to other Permian & Mesozoic sedimentary basins, adapted from Doré et al.,  
48 1999 and Naylor et al., 1999. Caledonian structural lineaments which segment the basins are  
49 lighted in red. **Abbreviations:** GGFZ, Great Glen Fault Zone; HBFC, Highland Boundary- Fair  
50 Head–Clew Bay Lineament; KBB, Kish Bank Basin; SUAG, Southern Uplands- Antrim-  
51 Galway Lineament; UB, Ulster Basin; WOB, West Orkney Basin; WSB, West Shetland Basin..  
52 **B)** Time structure map of the Base Permian or Variscan Unconformity in the Slyne Basin.  
53 Local sub-basins and structural elements are labelled. **Abbreviations:** CSTZ – Central Slyne  
54 Transfer Zone.

55 The Slyne Basin is a narrow chain of grabens and half-grabens that occupy the eastern margin  
56 of the Rockall Basin (Fig. 1). The Slyne Basin shows significant along-strike structural  
57 variability, with changes in dip direction of the kilometre-scale basin-bounding faults occurring  
58 over relatively short distances i.e. transfer zones. The transfer zones have been interpreted  
59 as areas where crustal-scale lineaments and terrane boundaries of Caledonian age transect  
60 the younger Late Palaeozoic and Mesozoic rifts. Similar phenomena have been observed in  
61 rift basins across the world, where pre-existing zones of weakness can be reactivated if  
62 oriented optimally. The north-western European Atlantic margin is underlain by a series of pre-  
63 existing structures and structural inheritance and reactivation has been well documented in  
64 the Norwegian and UK Atlantic margins (Doré et al., 1999; Doré et al., 2007; Ady & Whittaker,  
65 2019; Schiffer et al., 2019) as well as in the Iberian Atlantic margin (Alves et al., 2006; Pereira  
66 et al., 2017).

67 The structural geology of the Slyne Basin was the subject of significant study during the late  
68 1990s and early 2000s following the discovery of the Corrib gas field in 1996 (Dancer et al.,  
69 2005). Previous publications documented aspects of the structural evolution (Chapman et al.,  
70 1999; Dancer et al., 1999) and the role of exhumation in the petroleum system of the basin  
71 (Corocoran & Doré, 2002; Corocoran & Mecklenburgh, 2005), as well placing the basin in the  
72 regional context of the Irish Atlantic margin (e.g. Corfield et al., 1999; Walsh et al., 1999). In  
73 recent years, significantly more and higher quality seismic data, together with additional well  
74 data have been acquired throughout the Slyne Basin and neighbouring areas (Shannon,  
75 2018). Additionally, a comprehensive biostratigraphic study of all the Irish offshore basins has  
76 reclassified the ages of key syn-rift sequences (Merlin Energy Resources Consortium, 2020),  
77 warranting fresh investigation into the structural evolution of the Slyne Basin and its context  
78 within the greater Irish Atlantic margin.

79 This study utilizes an extensive database of borehole-constrained 2D and 3D seismic  
80 reflection data, coupled with the results from the new biostratigraphic database, to investigate  
81 the structural evolution of the Slyne Basin. Key aspects of this structural history, including the  
82 development of the major basin-bounding faults, the role of salt in basin evolution, and  
83 influence of pre-existing crustal-structures in the segmentation of the Slyne basin are



84 examined and characterised. These findings are then placed in a regional context to better  
85 understand the role of the Slyne Basin in the evolution of the greater Irish Atlantic margin.

### 86 3. Geological Setting

87 The Slyne Basin has a relatively flat present-day bathymetry, with water depths ranging from  
88 100 to 600m across most of the study area, with water depths increasing up to 2500m in the  
89 north (Dancer et al., 1999). It is divided into three distinct sub-basins: the Northern, Central  
90 and Southern Slyne sub-basins (Fig. 1, sensu Trueblood & Morton, 1991). These are  
91 separated by transfer zones (e.g. Morley et al., 1990; Gawthorpe & Hurst, 1993) which  
92 coincide with the location of major structural lineaments, in the form of Caledonian terrane  
93 boundaries.

94 The Slyne Basin is bounded along its eastern margin by the Irish Mainland Shelf, while the  
95 Porcupine and Slyne highs make up the western boundary (Fig. 1B). The Colm Basin,  
96 previously identified as a distinct Mesozoic basin (Dancer et al., 1999), appears to be an  
97 extension of the Northern Slyne Sub-basin, verging south-westwards between the Rockall  
98 Basin and the Porcupine High. A narrow, discontinuous basement horst which represents a  
99 southern extension of the Erris Ridge (Cunningham & Shannon, 1997) separates the Northern  
100 Slyne Sub-basin and the neighbouring Erris Basin from the Rockall Basin to the northwest.  
101 Similarly, a narrow basement high separates the Southern Slyne Sub-basin from the  
102 Porcupine Basin to the southwest.

#### 103 3.1. Basement configuration

104 Previous authors have noted the role of pre-existing Caledonian structures in the  
105 segmentation of younger Mesozoic basins on the Irish Atlantic margin, correlating the offshore  
106 extension of these crustal-scale structures with complex transfer zones separating distinct  
107 sub-basins (Trueblood & Morton, 1991; Dancer et al., 1999). Several authors have mapped  
108 the offshore extent of Caledonian structural lineaments on the Irish Atlantic margin (Lefort &  
109 Max, 1984; Tate, 1992; Naylor & Shannon, 2005; Štolfova & Shannon, 2009; Kimbell et al.,  
110 2010). There are three Caledonian structures relevant to the evolution of the Slyne Basin; the  
111 Great Glen Fault Zone (GGFZ), the Highland Boundary-Fair Head Clew Bay Fault Zone  
112 (HBFC) and the Southern Uplands-Antrim Galway Fault Zone (SUAG). The exact locations of  
113 these structures in the vicinity of the Slyne Basin are variably constrained; the NE-SW trending  
114 GGFZ has been mapped across the Irish Mainland Shelf to the west of the Erris Basin using  
115 deep seismic profiles and potential field datasets as a vertical strike-slip fault (Klemperer et  
116 al., 1991; Kimbell et al., 2010). The GGFZ intersects the Slyne Basin between the Northern  
117 and Central Slyne sub-basins at a location termed the Central Slyne Transfer Zone (CSTZ,

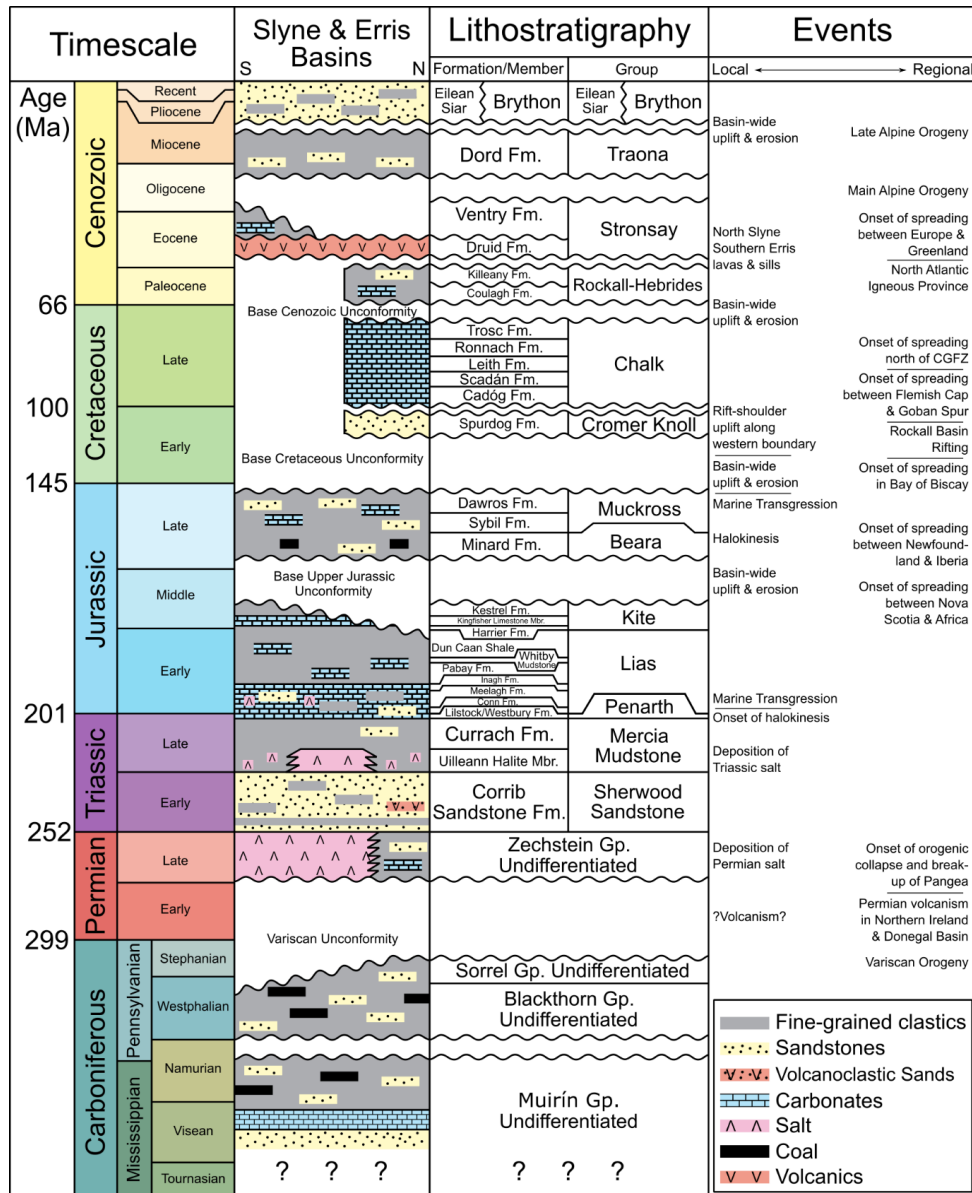


118 sensu Dancer et al., 1999). The HBFC and SUAG structures are more poorly constrained; the  
119 HBFC is an E-W oriented structure bounding the southern shore of Clew Bay on the west  
120 coast of Ireland and is mapped passing through Clare Island due west of Clew Bay (Fig. 1,  
121 Badley, 2001; Worthington & Walsh, 2011). The HBFC may correlate with the fault zone  
122 separating the Central and Southern Slyne sub-basins, but there is also evidence that splays  
123 of the HBFC may also be observed in the Central Slyne Sub-basin (Fig. 1B). The SUAG  
124 structure has been mapped trending E-W along the northern shore of Galway Bay (REF) and  
125 south of the Slyne Basin, through the Brendan Igneous Centre (Fig. 1). These lineaments  
126 separate different basement terranes which were assembled during the Caledonian Orogeny  
127 and have been extended from their known extents onshore Ireland and Scotland by several  
128 authors (e.g. Roberts et al., 1999; Tyrrell et al., 2007; Štolfová & Shannon, 2009). Limited pre-  
129 Carboniferous well penetrations in the Slyne Basin preclude the accurate mapping of these  
130 basement terranes and the interpretations of previous authors are adopted here.

### 131 3.2. Stratigraphic framework of the Slyne Basin

132 Previous stratigraphic nomenclature for the Slyne Basin was largely based on comparisons  
133 with the geology of the Hebridean basins exposed on the Isle of Skye (e.g. Trueblood &  
134 Morton; 1991). An updated stratigraphic nomenclature with revised biostratigraphy has  
135 recently been published, standardising nomenclature at group, formation and member levels  
136 across the sedimentary basins of the Irish Continental Shelf (Merlin Energy Resources  
137 Consortium, 2020). This stratigraphic nomenclature is used in this study (Fig. 2). The main  
138 Middle Jurassic syn-rift section of previous authors (e.g. Chapman et al., 1999; Dancer et al.,  
139 1999; Corcoran & Mecklenburgh, 2005; Dancer et al., 2005) has recently been reclassified as  
140 Late Jurassic in age. This has important implications for regional geodynamics which are  
141 discussed below. For full details on the biostratigraphic reclassification please refer to Merlin  
142 Energy Resources Consortium (2020).





143

144 **Figure 2:** Lithostratigraphic chart showing the simplified stratigraphy of the Slyne Basin, age  
 145 of key horizons, and typical seismic stratigraphy from the Central Slyne Sub-Basin. Adapted  
 146 from Merlin Energy Resources Consortium, 2020.

147 The pre-rift section of the Slyne Basin consists of Carboniferous mudstones and sandstones  
 148 with interbedded layers of coal, underlain by Silurian and older metasediments (Merlin Energy  
 149 Resources Consortium, 2020). This is overlain by an evaporite-rich Permian sequence which  
 150 is a lateral equivalent of the Zechstein Group encountered throughout NW Europe (O'Sullivan



151 et al., 2021). The overlying Triassic section is sub-divided into Lower Triassic fluvial  
152 sandstones and Upper Triassic playa, sabkha and lacustrine mudstones and claystones  
153 interbedded with thin limestone, sandstone, and anhydrite beds (Dancer et al., 2005; Štolfova  
154 & Shannon, 2009). A massive halite unit is present at the base of the Upper Triassic section  
155 in the northern Slyne Basin but is absent in the central and southern parts of the basin  
156 (O'Sullivan et al., 2021).

157 The Lower Jurassic section is composed of marine sandstone, mudstones and carbonates,  
158 overlain by Middle Jurassic calcareous marine mudstones (Trueblood & Morton, 1991; Dancer  
159 et al., 1999). The Kingfisher Limestone Member is a unit of thick limestones that occurs at the  
160 base of Kestrel Formation (sensu Merlin Energy Resources Consortium, 2020) and which  
161 forms a distinct, semi-regional seismic marker termed the 'Bajocian Limestone Marker' in  
162 previous literature (e.g. Trueblood & Morton, 1991; Scotchman & Thomas, 1995; Dancer et  
163 al., 1999). A regional unconformity separates the underlying Lower and Middle Jurassic  
164 sections from the overlying Upper Jurassic sediments. The Upper Jurassic section consists of  
165 terrestrial and fluvio-estuarine mudstones and sandstones with numerous palaeosols and coal  
166 layers, which are overlain by the marine mudstones, indicating a regional marine transgression  
167 occurred during the late Oxfordian to Tithonian (Merlin Energy Resources Consortium, 2020).

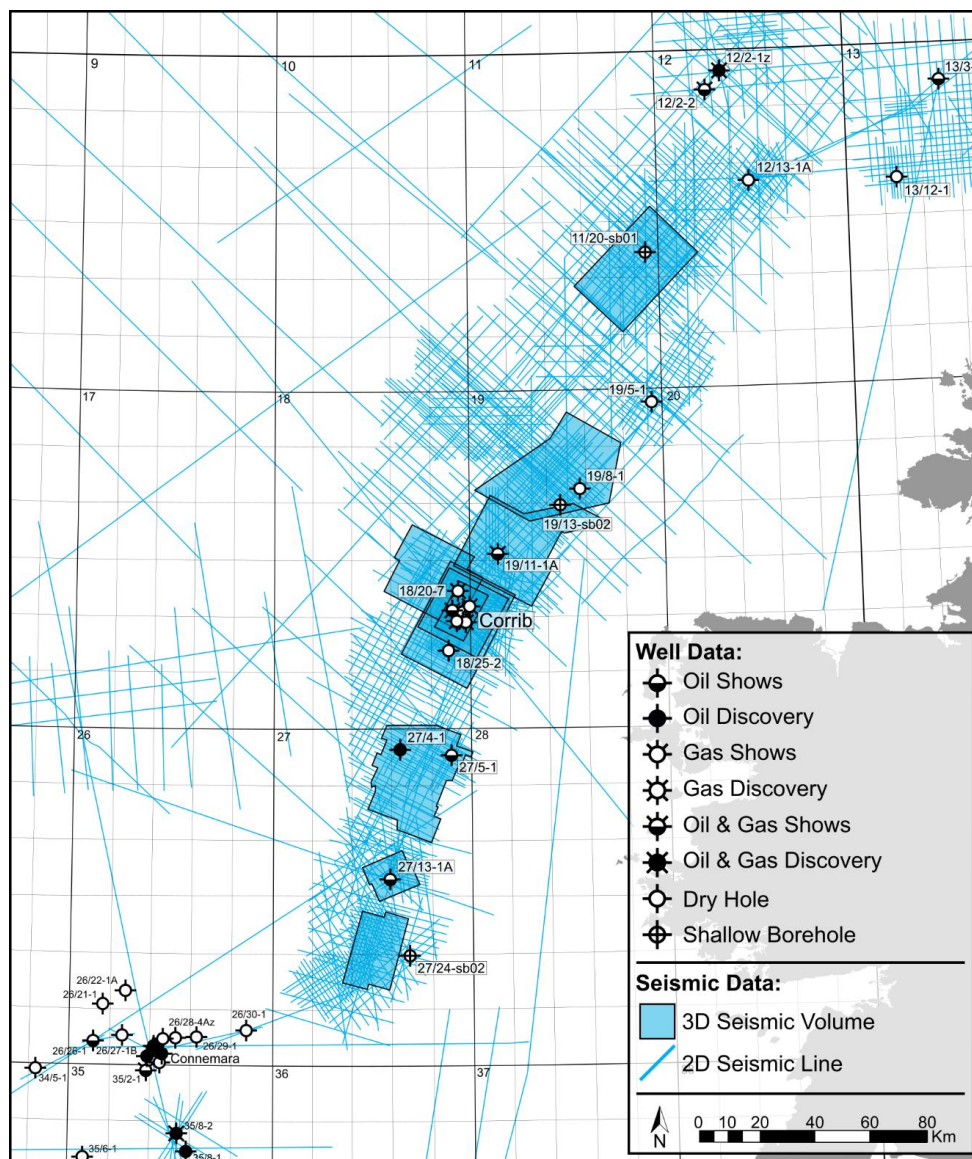
168 The Base-Cretaceous Unconformity separates the Cretaceous section of the Slyne Basin from  
169 the underlying Jurassic strata. The Lower Cretaceous stratigraphy consists of Albian-aged  
170 glauconitic mudstones and sandstones, while the overlying Upper Cretaceous section is  
171 composed of limestones and calcareous mudstones. The Base-Cenozoic Unconformity forms  
172 the lower boundary to the Cenozoic succession in the Slyne Basin. The Cenozoic section can  
173 be subdivided into three sequences: a layer of Eocene lava locally developed in the northern  
174 and southern areas of the Slyne Basin, overlain by an Eocene-Miocene section and a Miocene  
175 to Quaternary section, both consisting of poorly consolidated marine mudstones and  
176 sandstones, separated by a mid-Miocene unconformity.





#### 177 4. Dataset & Methodology

178 This study focused on the interpretation of an extensive suite of multi-vintage 2D and 3D  
179 seismic reflection data collected during hydrocarbon exploration in the Slyne Basin (Fig. 3).  
180 The 2D seismic dataset consists of 17 surveys acquired between 1980 and 2007, comprising  
181 over 22,000 line-kilometres of data, while the 3D seismic dataset consists of eight surveys  
182 acquired between 1997 and 2013 and covers almost 4,000 square-kilometres. Seismic data  
183 quality varies from very poor to good, with the more modern vintages typically providing clearer  
184 imaging. Data quality in the Slyne Basin is heavily influenced by the near-seabed geology,  
185 with the distribution of Cenozoic lava flows and intrusive sills, coupled with Cretaceous chalk  
186 causing imaging problems including multiples, energy scattering and signal attenuation  
187 (Dancer & Pillar, 2001). These problems are most severe in the Northern Slyne Sub-basin,  
188 and the western margin of the Southern Slyne Sub-basin. The application of modern  
189 processing techniques and use of 3D seismic data has improved data quality in the region  
190 somewhat (Dancer & Pillar, 2001; Droujinine et al., 2005; Rohrman, 2007; Hardy et al., 2010),  
191 most recently with the acquisition of an ocean-bottom cable survey over the Corrib gas field  
192 in 2012 and 2013 (Shannon, 2018). Seismic sections are presented in European polarity  
193 (Brown, 2001), where a positive downwards increase in acoustic impedance corresponds to  
194 a positive (red) reflection event and a decrease corresponds to a negative (blue) reflection  
195 event. All sections are vertically exaggerated by a factor of three and ball-ends are used to  
196 highlight where a fault terminates within a certain stratigraphic package, while faults without  
197 ball-ends are truncated by a younger unconformity.



198

199 **Figure 3:** Map showing study area and data sets used.

200 Thirteen key horizons were mapped across the Slyne Basin in the time domain (Fig. 2). The  
 201 ages of these horizons were constrained using exploration and appraisal wells in addition to  
 202 shallow boreholes. The Northern Slyne Sub-basin has the highest well density, including eight  
 203 appraisal and production wells associated with the Corrib gas field, and four near-field  
 204 exploration wells (19/8-1, 19/11-1A, 18/20-7 and 18/25-2), with a further three exploration  
 205 wells in the Central Slyne Sub-basin (27/4-1, 27/5-1 and 27/13-1). The stratigraphy of the  
 206 Southern Slyne Sub-basin is unconstrained except for a single shallow borehole (27/24-

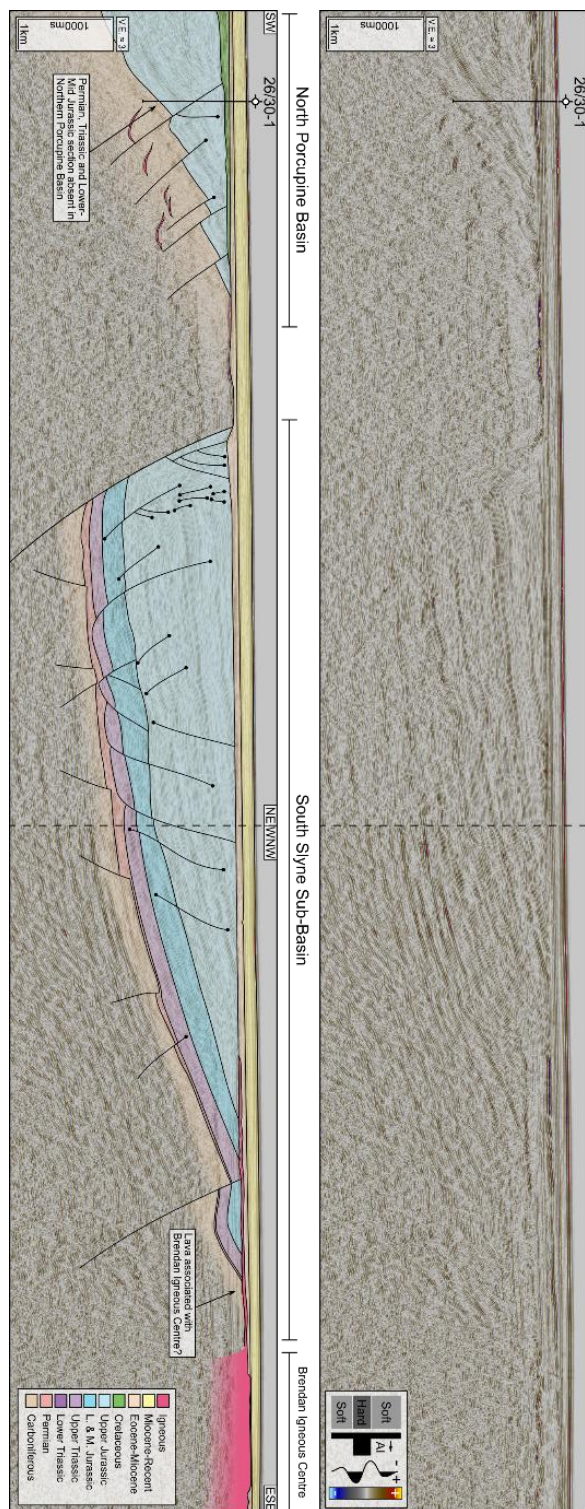


207 sb02A) which proved Lower Jurassic and Upper Triassic sediments beneath the Base-  
208 Cenozoic Unconformity (Fugro, 1994a). The dataset associated with the exploration, appraisal  
209 and production wells consist of comprehensive suites of wireline logs (gamma, caliper,  
210 neutron-density, sonic, and resistivity logs), well completion reports with formation tops, and  
211 time-depth relationship data as either checkshots, or vertical seismic profiles (VSPs).

## 212 5. Results

### 213 5.1. Basin geometry & transfer zones

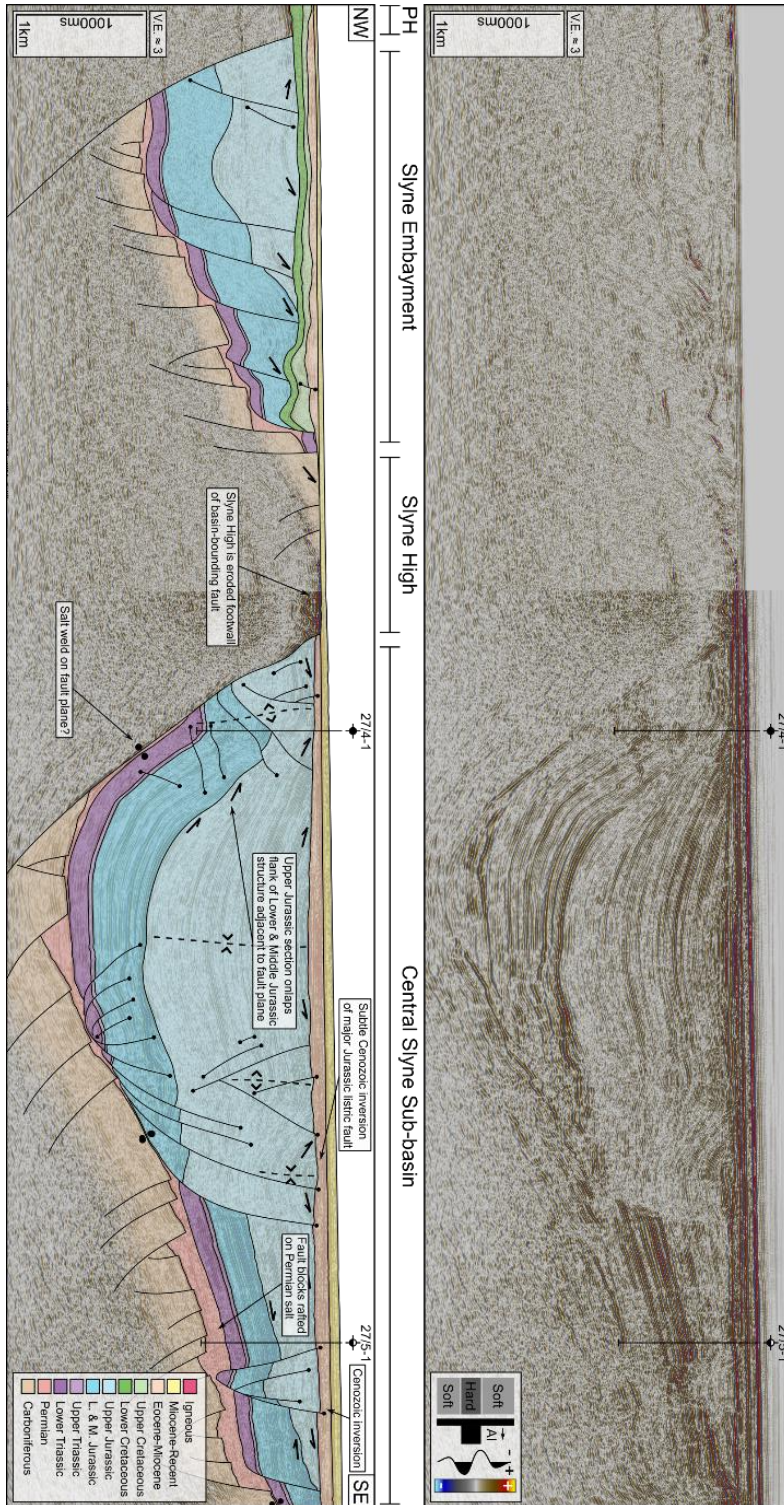
214 The Southern and Central sub-basins are half-grabens which dip towards the northwest (Fig.  
215 4 & 5), with a NNE-SSW oriented basin-bounding fault separating them from the Porcupine  
216 High to the west. As no Permian or Mesozoic strata are preserved on the footwall of these  
217 basin-bounding faults (the Porcupine High) either through non-deposition or erosion (Fig. 4 &  
218 5), the total throw on these faults is difficult to constrain. Nevertheless, the elevation of the  
219 Base-Permian Unconformity in the adjacent hanging wall provides a minimum throw estimate  
220 of 3000 ms TWTT (two-way travel time) along most of the length of this fault (Fig. 1B). Unlike  
221 its Southern and Central neighbours, the Northern Slyne Sub-basin is an eastward-dipping  
222 graben (Fig. 6 & 7) bounded by a series of segmented faults along its eastern boundary with  
223 the Irish Mainland Shelf (Fig. 1B), while a narrow basement horst separates it from the Rockall  
224 Basin to the NW. The fault system bounding the eastern margin of the Northern Slyne Sub-  
225 basin consists of a series of left-stepping, NE-SW oriented faults linked by relay ramps (Fig.  
226 1B). These faults are of a similar scale to the fault bounding the Southern and Central sub-  
227 basins, with over 3000 ms TWTT of throw recorded (Fig. 1B). The northernmost segment of  
228 this fault system separates the Slyne Basin from the Erris Basin to the north, with the Erris  
229 Basin being downthrown relative to the Northern Slyne Sub-basin across this fault (Fig. 8).





231 **Figure 4:** Composite section of 2D seismic lines NWI-93-202 and NWI-93-028 and  
232 accompanying geoseismic interpretation covering the Southern Slyne sub-basin, North  
233 Porcupine Basin, and Brendan Igneous Centre. The Southern sub-basin is a westward-  
234 dipping half-graben, and is downthrown relative to the North Porcupine Basin, separated by a  
235 narrow high composed of crystalline basement. See Figure 1 for location.

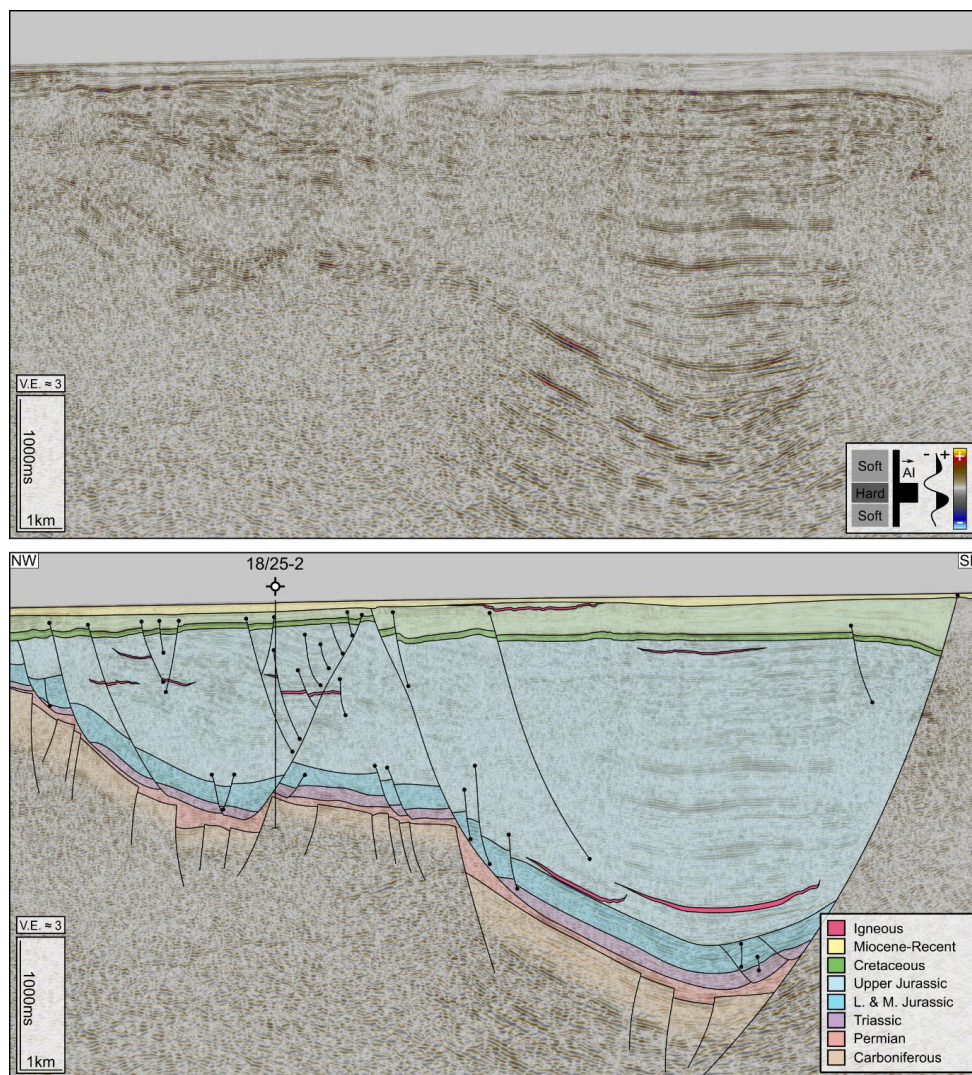








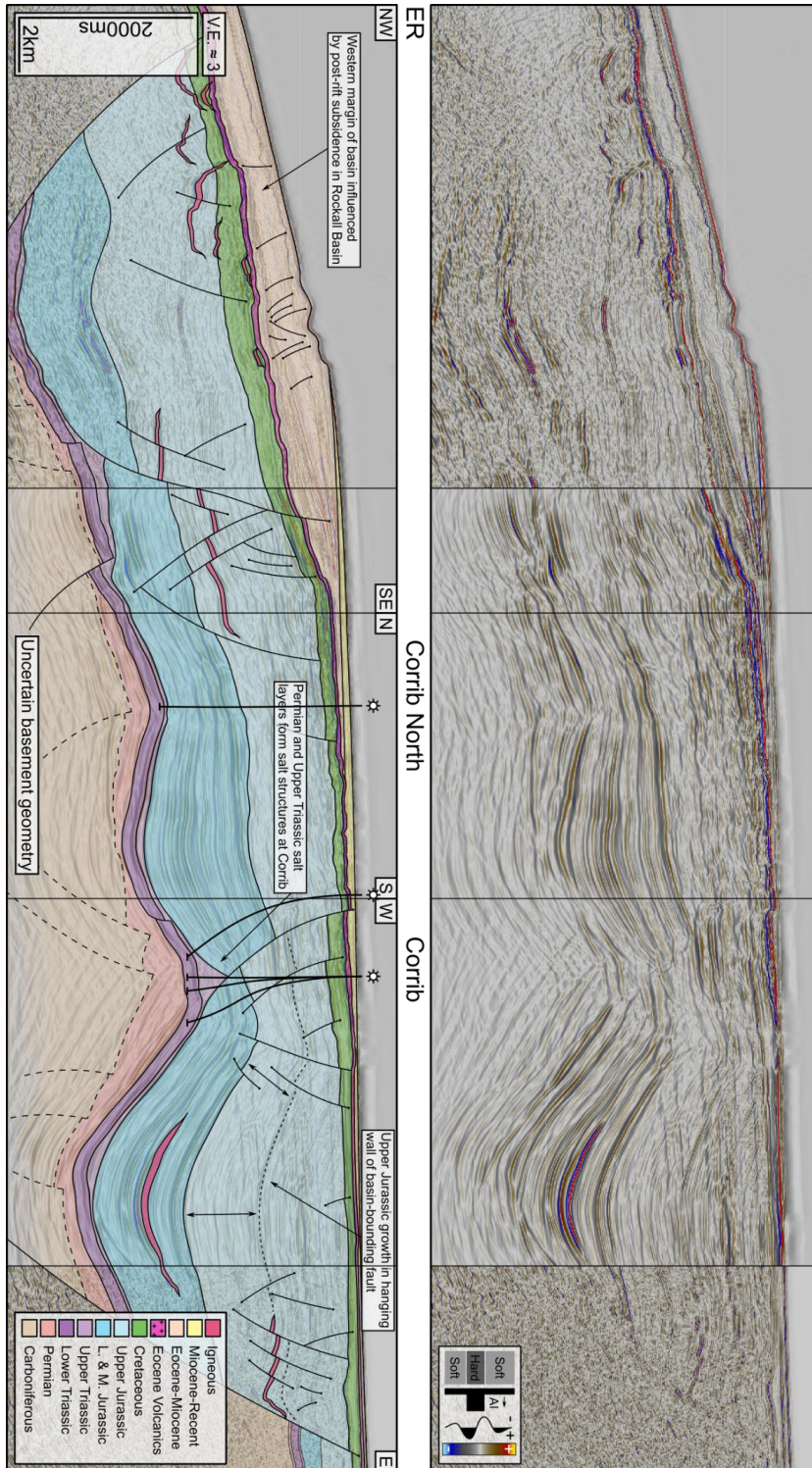
237 **Figure 5:** Composite seismic section of 2D seismic line E96IE09- 28 and inline 2740 from the  
238 2000/08 (E00IE09) 3D seismic volume from the Central Slyne Sub-basin, with accompanying  
239 seismic interpretation. See Figure 1 for location. **Abbreviations:** PH – Porcupine High.



240

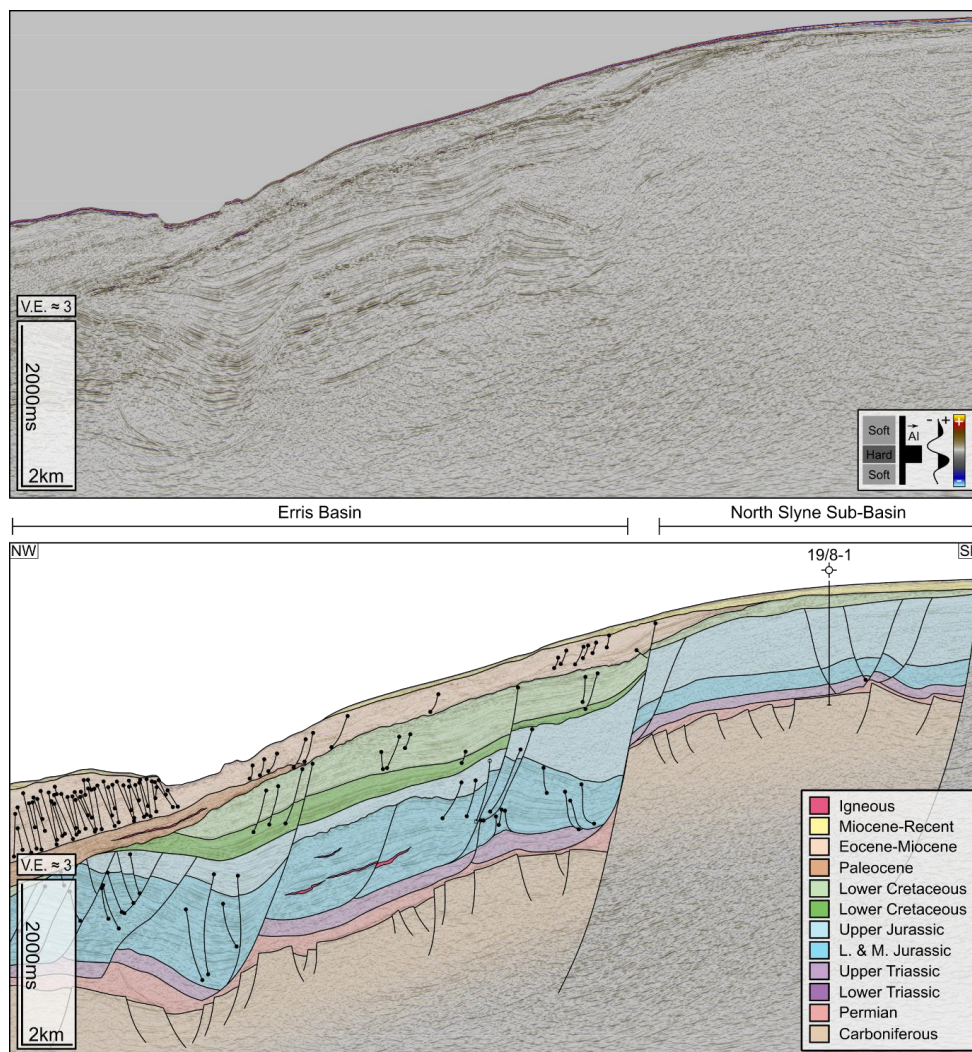
241 **Figure 6:** 2D seismic line E93IE07 and accompanying geoseismic interpretation from the  
242 Central Slyne Transfer Zone. Basin polarity has switched from the westward-dipping half-  
243 graben geometry of the Central and Southern sub-basins to an eastward-dipping half-graben  
244 geometry. The presence of near-seabed Upper Cretaceous Chalk causes a significant  
245 reduction in image quality. See Figure 1 for location.







247 **Figure 7:** Composite section of an arbitrary line from the Iniskea 2018 3D volume and 2D  
248 seismic line ST9808-1002 from the Northern Slyne sub-basin, and accompanying geoseismic  
249 interpretation. Significantly thicker Zechstein salt in this part of the Slyne Basin forms salt-  
250 pillows and salt-anticlines, folding the overlying Mesozoic section. Detachment on the Uilleann  
251 Halite causes rafting and listric faulting in the overlying Jurassic section. See Figure 1 for  
252 location. **Abbreviations:** ER – Erris Ridge.



253

254 **Figure 8:** 2D seismic line ST9505-430 and accompanying geoseismic interpretation covering  
 255 the Northern Slyne sub-basin and the southern Erris Basin. The Erris Basin is downthrown  
 256 relative to the Slyne Basin, and has a significantly thicker Lower and Middle Jurassic section  
 257 preserved, but conversely reduced Upper Jurassic stratigraphy. Significantly thicker  
 258 Cretaceous and Cenozoic post-rift stratigraphy is preserved in the Erris Basin relative to the  
 259 Slyne Basin. See Figure 1 for seismic line location.

260 The reversal of basin polarity occurs across the CSTZ, which coincides with the intersection  
 261 of the offshore extension of the GGFZ and the Slyne Basin. Deep seismic transects adjacent  
 262 to the Slyne Basin image the GGFZ as a NE-SW trending vertical discontinuity which appears  
 263 to offset the Moho (Klemperer et al., 1991). The throw on the basin-bounding faults north and  
 264 south of the CSTZ rapidly decreases as they approach the CSTZ so that horizons are  
 265 continuous between the basins and strain is transferred between the faults of opposed polarity





266 via a convergent, conjugate transfer zone (sensu Morley et al., 1990). Both faults have over  
267 3000 ms TWTT of throw on the Base Permian Unconformity within 10 kilometres of the CSTZ  
268 (Fig. 1, 5, 6), with this value likely being an underrepresentation of the true throw given the  
269 kilometre-scale erosion of Jurassic sediments recorded both north and south of the CSTZ  
270 beneath the post-rift unconformities (e.g. Corcoran & Mecklenburgh, 2005; Biancotto et al.,  
271 2007). In addition to the faults bounding the Central and Northern Slyne sub-basins, a NE-SW  
272 oriented, southward dipping fault bounds the Slyne Embayment, a small half-graben to the  
273 southwest of the CSTZ (Fig. 1B, 5). This suggests that the GGFZ acted as a barrier to the  
274 propagation of the basin-bounding fault systems to both the north and south. The GGFZ is  
275 likely linked to both the fault bounding the Slyne Embayment and the southernmost segment  
276 of fault system bounding the Northern Slyne Sub-basin, both of which are subparallel to this  
277 major regional structure.

278 The HBFC fault is interpreted as a hard-linked NE-SW oriented fault, dipping towards the NW,  
279 which downthrows the Central Slyne Sub-basin relative to the Southern Slyne Sub-basin (Fig.  
280 1B). The HBFC fault also appears to offset the NNE-SSW oriented fault bounding the Central  
281 and Southern Slyne sub-basins (Fig. 1B), which may be a product of both normal dip-slip  
282 movement observed offshore on seismic data and strike-slip movement recorded onshore  
283 Ireland (e.g. Worthington & Walsh, 2011; Anderson et al., 2018). The nature of the interaction  
284 between these two faults is unclear due to poor seismic image quality caused by shallow  
285 Cenozoic lavas which blanket the western margin of the Southern Slyne Sub-basin. However,  
286 the lateral offset of the NE-SW oriented basin-bounding fault and the adjacent Porcupine High  
287 either side of the FHCB fault is well imaged on seismic sections immediately north and south  
288 of this zone.

## 289 5.2. The role of salt in basin development

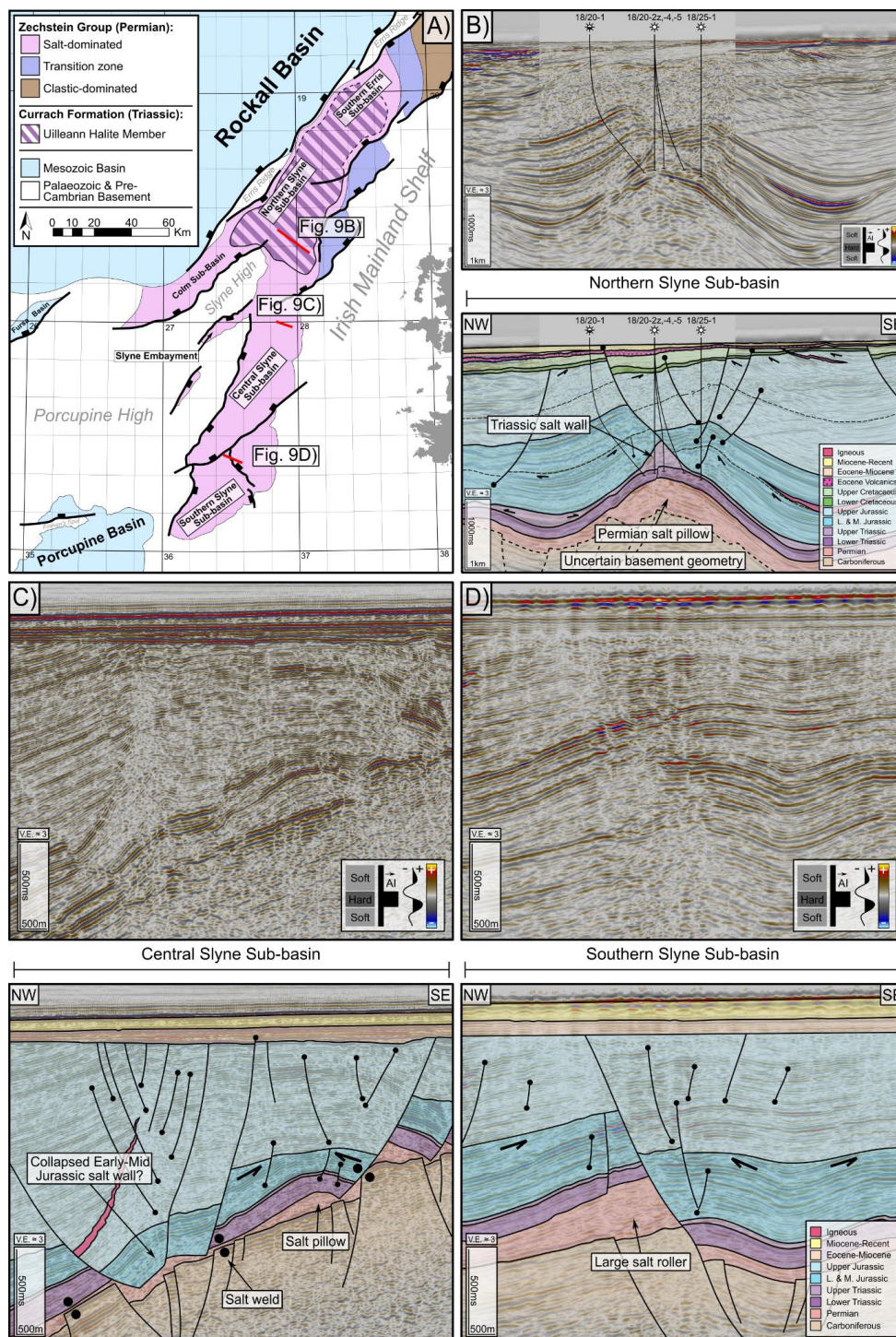
290 The Slyne Basin contains two layers of salt; the Permian Zechstein Group and the Upper  
291 Triassic Uilleann Halite Member (Fig. 2; Dancer et al., 2005; Merlin Energy Resources  
292 Consortium, 2020; Fig. 2). The Zechstein Group is composed predominately of halite and  
293 gypsum, while the Uilleann Halite Member is composed predominantly of halite interbedded  
294 with red mudstone and anhydrite (O'Sullivan et al., 2021).

295 In the Central and Southern sub-basins, south of the CSTZ, only the Zechstein Group salt is  
296 present (Fig. 2), where it mechanically detaches the sub-salt basement from the Mesozoic  
297 supra-salt basin-fill (Fig. 4-5, 9, 10). Several halokinetic structures are present in the Central  
298 and Southern Slyne sub-basins, including large salt rollers, collapsed diapirs and rafted fault  
299 blocks (Fig. 5, 9). There are also several high-relief monoclines adjacent to the basin-bounding  
300 fault in the Central Slyne Sub-basin which have been noted by previous authors (Fig. 5;





301 Dancer et al., 1999). The Triassic and Lower-Middle Jurassic section in these structures is  
302 encountered at a similar depth to the same section along the eastern margin of the basin, and  
303 the Triassic section appears to have welded to the crystalline basement of the Porcupine High  
304 across the fault plane of the basin-bounding fault (Fig. 5). These structures likely formed  
305 initially as forced folds above the sub-salt basin-bounding faults during the early stages of  
306 rifting in the Late Jurassic, resulting in the Upper Jurassic section onlapping the flank of these  
307 structures. As extension continued the fault breached the salt and led to the present geometry  
308 (O'Sullivan et al., 2021).





310 **Figure 9:** Seismic sections and accompany interpretations showing salt structures in the Slyne  
311 Basin. **A)** Map showing the distribution of Upper Triassic and Permian salt in the Slyne Basin.  
312 Adapted from O'Sullivan et al., 2021. **B)** Seismic and geoseismic section through the Corrib  
313 gas field showing the kinematic interaction between Upper Triassic and Permian salt. The  
314 Permian salt forms a NE-SW oriented salt pillow, while the Upper Triassic forms an elongate  
315 salt wall parallel to the fold-axis of the salt pillow. Adapted from O'Sullivan & Childs, 2021. **C)**  
316 Several salt-related structures in the Central Slyne Sub-basin, including a salt pillow, salt roller  
317 and an apparent collapsed salt diapir. **D)** A large salt roller from the Southern Slyne Sub-basin.  
318 The fault in the supra-salt section appears to have hard-linked with the sub-salt basement  
319 fault.

320 In the Northern sub-basin both the Permian and Upper Triassic salt layers are present (Fig.  
321 9A; Corcoran & Mecklenburgh, 2005; O'Sullivan et al., 2021). Here, both layers mechanically  
322 detach the stratigraphy above and below them, with the Permian salt detaching the Lower  
323 Triassic from the Carboniferous basement, while the Upper Triassic salt detaches the Jurassic  
324 section from the Lower Triassic (Fig. 7, 9B). Halokinetic structures formed in the Permian and  
325 Triassic salts are often coincident and can be demonstrated to be kinematically related. This  
326 is exemplified by the structure containing the Corrib gas field (Fig. 7, 9; Corcoran &  
327 Mecklenburgh, 2005; Dancer et al., 2005); here, the Permian salt forms a NE-SW trending  
328 salt pillow, which folds the overlying Mesozoic sediments. An Upper Triassic salt wall formed  
329 parallel to the fold-axis of the Permian salt pillow and forms the footwall to a listric delamination  
330 fault which downthrows the folded Jurassic section to the SE (Fig. 7, 9B). The evolution of the  
331 Corrib gas field is discussed in detail in O'Sullivan & Childs (2021).

332 Several of the halokinetic structures in the Slyne Basin record several discrete periods of  
333 growth and development. There is significant evidence for halokinesis during the Early and  
334 Middle Jurassic, with the crests of fault-blocks cored by salt rollers eroded by the base-Upper  
335 Jurassic Unconformity. There is also evidence for Permian salt diapirs forming in the Central  
336 Slyne Sub-basin during the Early to Middle Jurassic which collapsed during the Late Jurassic  
337 extensional episode, as recorded in the reduced Lower and Middle Jurassic section observed  
338 in narrow fault-bounded grabens (e.g. Fig. 9C; Vendeville & Jackson, 2001; O'Sullivan et al.,  
339 2021). Several other halokinetic structures were also reactivated during Late Jurassic  
340 extension, including the structure containing the Corrib gas field, with significant Late Jurassic  
341 throw recorded on the listric fault above the Triassic salt wall (Fig. 9B). Some of these salt  
342 structures have also undergone minor modification during the Cretaceous and Cenozoic.

343



## 344 6. Structural Evolution of the Slyne Basin

### 345 6.1. Permian and Triassic

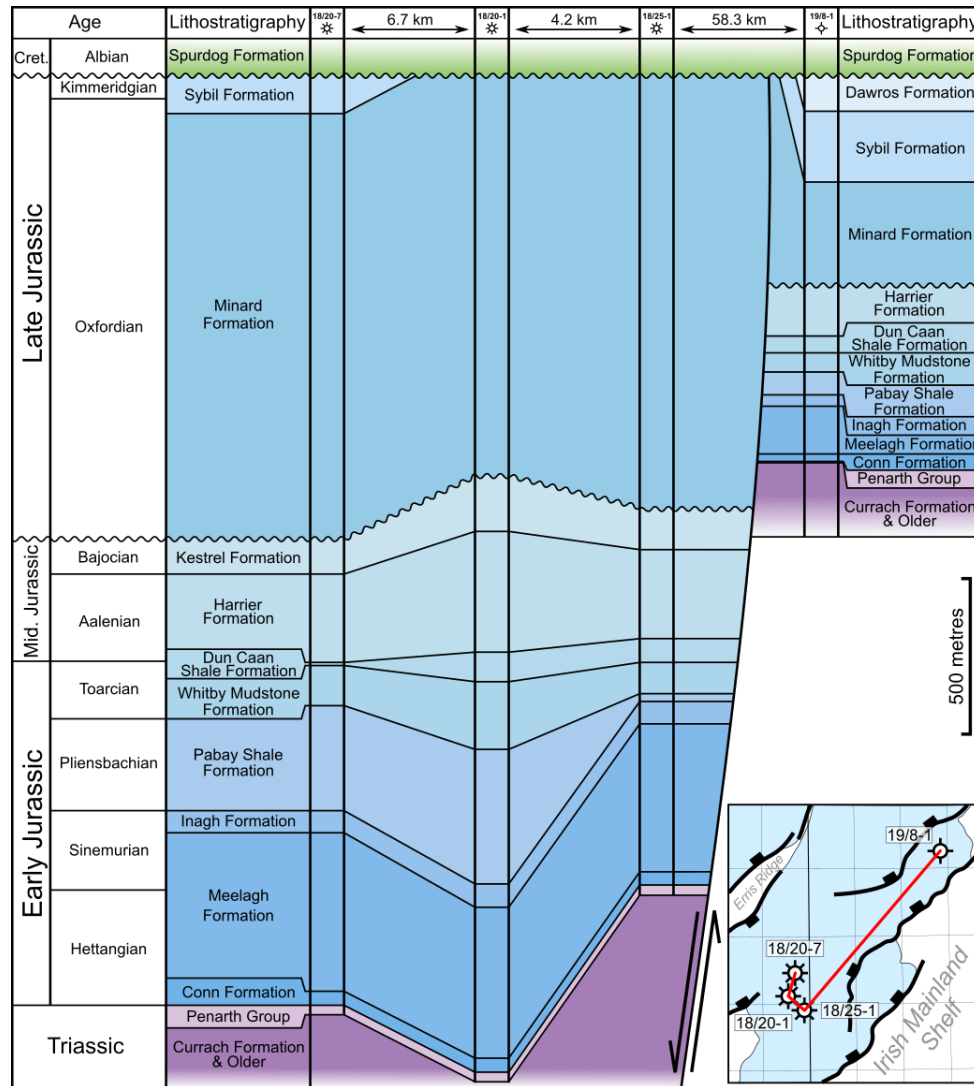
346 Post-Variscan extension began in the Slyne Basin during the Late Permian. Several hundred  
347 metres of Zechstein halite was deposited throughout the Slyne Basin (Fig. 9A), likely in fault-  
348 bounded depocentres (O'Sullivan et al., 2021). The Permian boundaries of the Slyne Basin  
349 are poorly understood due to post-Permian halokinesis, but it is clear that the Slyne Basin was  
350 an area of active extension, relative to the neighbouring Erris and Porcupine basins, with a  
351 thin (10s of metres thick) layer of predominately clastic and carbonate facies developed in the  
352 former (Robeson et al., 1988; O'Sullivan et al., 2021), and no evidence of Permian sediments  
353 in the latter (Jones & Underhill, 2011; Bulois et al., 2018).

354 The Triassic was a period of relative quiescence in the Slyne Basin, typified by the near  
355 isopachous nature of the Lower Triassic section throughout the basin (Fig. 5, 7, 9). The local  
356 thickening of the Upper Triassic section in the synclines flanking the Corrib anticline (Fig. 7,  
357 9B) suggest that low-strain extension may have begun during the Late Triassic, at least in the  
358 Northern Slyne Sub-basin (O'Sullivan & Childs, 2021).

### 359 6.2. Early and Middle Jurassic

360 Low-strain regional extension occurred throughout the Slyne Basin during the Early and  
361 Middle Jurassic. The Lower and Middle Jurassic section can be observed thickening towards  
362 the basin-bounding faults in the Central Slyne Sub-basin by a few 10s of ms TWTT (10-100  
363 metres), but this shape is accentuated by erosion of this section at the Base Upper Jurassic  
364 Unconformity on the basin margins (e.g. well 27/5-1 location in Fig. 5). The Lower and Middle  
365 Jurassic section is also observed thickening into the synclines flanking the salt-cored folds in  
366 the Northern Slyne Sub-basin (Fig. 7, 9B), indicating the Permian salt was undergoing  
367 halokinesis during this period (O'Sullivan & Childs, 2021). There is also evidence of salt walls  
368 forming in the Central Slyne Sub-basin during the Early to Middle Jurassic along with large  
369 salt rollers beneath active listric faults soling out in the Permian Zechstein Group (Fig. 9C, D).  
370 In the Northern Slyne Sub-basin, a comparison of the stratigraphic section encountered in  
371 basinward wells with the single available well located on the footwall of the basin-bounding  
372 faults demonstrates the growth in the Lower and Middle Jurassic section during this period of  
373 regional extension (Fig. 10).





374

375 **Figure 10:** Well correlation through the Jurassic section of key wells from the Northern Slyne  
 376 Sub-basin, highlighting thickness variations in the Lower and Middle Jurassic section between  
 377 wells within the basin and the 19/8-1 well on the footwall of the basin-bounding fault system.

378 A regional unconformity separates the Lower to Middle Jurassic from the Upper Jurassic  
 379 section throughout the Slyne Basin, termed the Base Upper Jurassic Unconformity. This  
 380 unconformity can be quite rugose on the margins of the basins, such as the area around the  
 381 27/5-1 well in the Central Slyne Sub-basin (Fig. 5), while being a relatively flat paraconformity  
 382 in the centre of the basin (e.g. Fig. 5, 7). There are several angular truncations observed  
 383 throughout the Slyne Basin at the base of this unconformity, particularly above salt-related  
 384 structures formed during Early to Middle Jurassic extension, including footwalls above salt

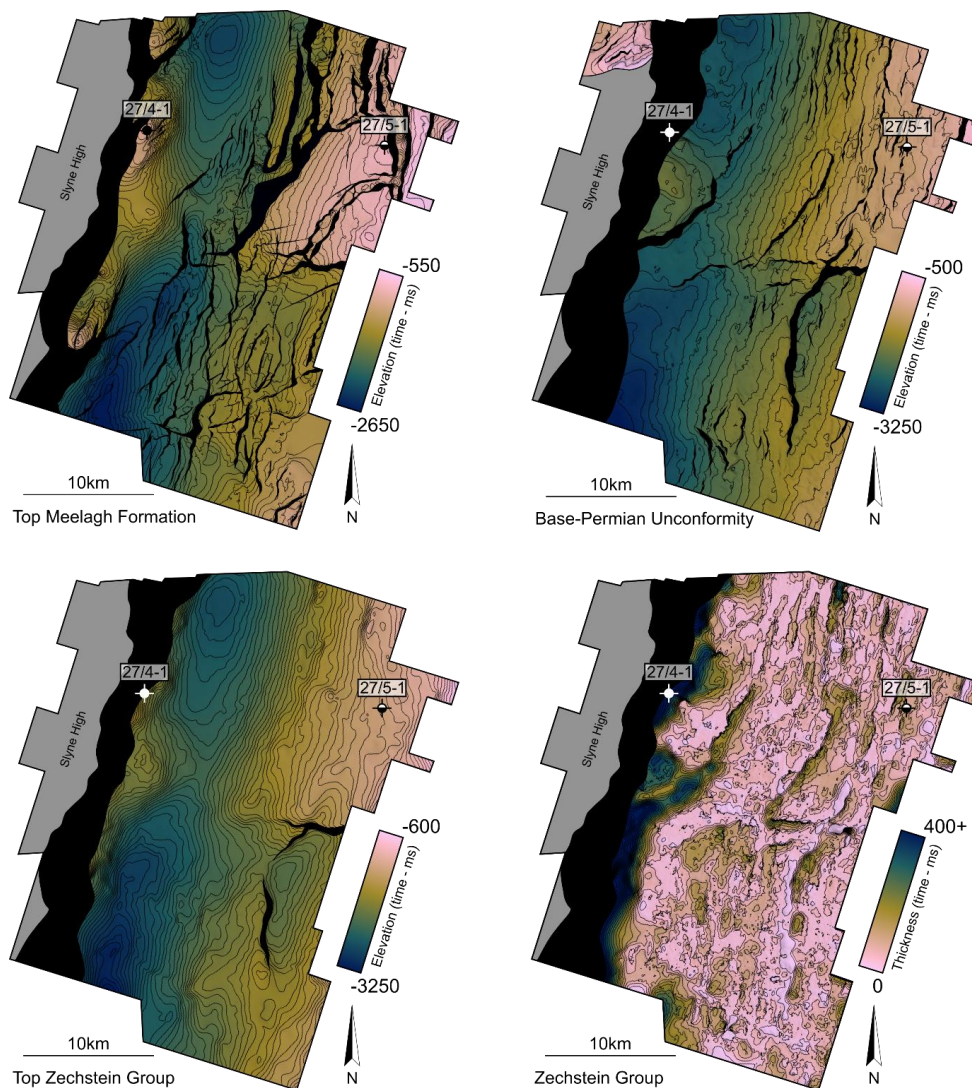


385 rollers and the crests of folds above salt pillows (Fig. 9C, D). Throughout the Slyne Basin the  
386 late Middle Jurassic (Bathonian and Callovian) section is absent at this unconformity, either  
387 through erosion or non-deposition (Merlin Energy Resources Consortium, 2020). The exact  
388 cause of this unconformity is difficult to constrain, although some authors have suggested  
389 thermal doming and dynamic topography above a mantle plume similar to that implicated in  
390 the North Sea (Tate & Dobson, 1989; Underhill & Partington, 1993; Doré et al., 1999).

### 391 6.3. Late Jurassic

392 The main phase of extension commenced during the Late Jurassic, with the basin-bounding  
393 faults accumulating several kilometres of throw during this extensional episode along with the  
394 deposition of several kilometres of Upper Jurassic sediment (Fig. 4-8). Despite this, there are  
395 no obvious growth sequences observed in the Southern Slyne Sub-basin (Fig. 4) or in the  
396 southern portion of the Northern Slyne Sub-basin (Fig. 6). Growth sequences are observed in  
397 the hanging walls of the bounding faults in the Northern Slyne Sub-basin with reflectors  
398 diverging towards the SE (Fig. 7). In the Central Slyne Sub-basin, the Upper Jurassic section  
399 onlaps the flank of the high-relief monocline in the immediate hanging wall of the basin-  
400 bounding fault and thickens into the hanging wall of major intra-basinal listric fault (Fig. 5).  
401 This stratal geometry, along with a similar thickness of Lower-Middle Jurassic sediment  
402 present in the neighbouring Slyne Embayment, suggests that most of the throw on this fault  
403 accumulated during the Late Jurassic, with the kilometre-scale post-rift uplift and erosion  
404 during the Cretaceous and Cenozoic removing any Jurassic sediment from the intervening  
405 footwall, forming the Slyne High (Fig. 5). The presence of NE-SW oriented fault splays in the  
406 sub-salt hanging wall of this fault (e.g. Fig. 11) suggests that the large NNE-SSW oriented  
407 fault bounding the Central and Southern Slyne Sub-basins formed through the linkage of NE-  
408 SW oriented fault segments, likely during this Late Jurassic phase of rifting.





409

Top Zechstein Group

Zechstein Group

410 **Figure 11:** Surfaces from the E00IE09 3D seismic volume from the Central sub-basin **A)**  
 411 TWTT structure map of the Top Meelagh Formation. Several high-relief anticlinal closures are  
 412 present in the immediate hanging-wall of the basin-bounding fault, including the structure  
 413 containing the 27/4-1 'Bandon' oil accumulation. **B)** TWTT structure map of the Variscan  
 414 Unconformity. Notice the significant differences in fault pattern between the Variscan  
 415 Unconformity (pre-salt) and Top Meelagh Formation (post-salt). **C)** TWTT structure map of the  
 416 Top Zechstein Group. Notice the lack of faulting on this surface. **D)** TWTT thickness map  
 417 (isochron) of the Zechstein Group. The Zechstein salt is thinned throughout most of the survey  
 418 area, with numerous apparent welds formed between the post- and pre-salt sections. The  
 419 Zechstein salt is overthickened in the immediate hanging wall of the basin-bounding fault.

420 Two discrete phases of Late Jurassic extension have been identified in the neighbouring  
 421 Porcupine Basin, the first occurring in the Oxfordian and the second in the Kimmeridgian



422 (Saqab et al., 2020). Both of these extensional episodes may have also occurred in the Slyne  
423 Basin but, unlike the Porcupine Basin, a significant section of the Late Jurassic syn-rift section  
424 was subsequently removed during post-rift uplift and erosion (e.g. Corcoran & Mecklenburgh,  
425 2005) and evidence of a second phase may have been removed.

426

#### 427 6.4. Cretaceous and Cenozoic

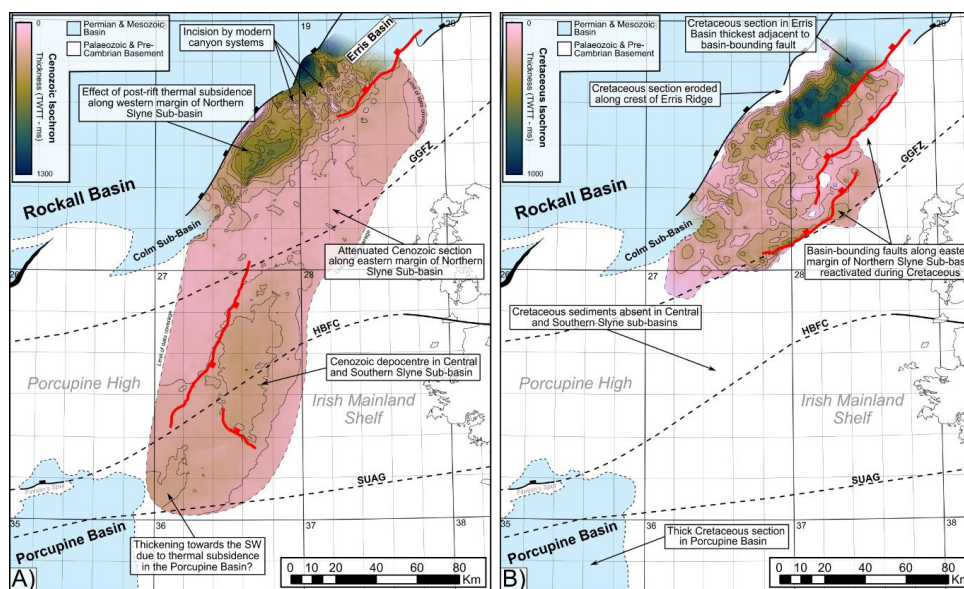
428 The Slyne Basin experienced kilometre-scale uplift and erosion at the end of the Jurassic and  
429 during the Early Cretaceous, removing a significant section of the Upper Jurassic syn-rift  
430 section throughout the basin (Table 1). The majority of the Slyne Basin was likely a  
431 topographic high relative to surrounding regions during the Cretaceous, including the Erris,  
432 Porcupine and Rockall basins (Fig. 8; Musgrove & Mitchener, 1996; Chapman et al., 1999;  
433 Saqab et al., 2020). Up to 400 metres of Albian and Late Cretaceous sediments were  
434 deposited in the Northern Slyne Sub-basin and the Slyne Embayment (5-8, 12B), and possibly  
435 in the Central and Southern Slyne sub-basins. Several syn-rift faults were reactivated during  
436 the Cretaceous, with both normal and reverse movement observed throughout the Slyne  
437 Basin. In the Northern Slyne Sub-basin the main delamination fault above the Corrib anticline  
438 has a significant Cretaceous growth sequence that thickens from 200 ms TWTT (c. 150 m) in  
439 the footwall to over 400 ms TWTT (c. 380 m) in the hanging-wall (Fig. 7). Additionally, the  
440 individual segments of the basin-bounding fault system along the eastern margin of the  
441 Northern Slyne Sub-basin were reactivated during the Cretaceous (Fig. 12B). The throw on  
442 the northern segment varies from 30-100 ms TWTT adjacent to the Corrib gas field through to  
443 the 19/8-1 well (Fig. 7, 8) while on the segment to the south adjacent to the 18/25-2 well (Fig.  
444 6) the throw locally exceeds 300 ms TWTT. In addition to these major faults, several smaller  
445 faults offset the Cretaceous section throughout the Northern Slyne Sub-basin with the majority  
446 of these faults having throws less than 100 ms TWTT (Fig. 6, 7). The fault bounding the Slyne  
447 Embayment appears not to have been active during this time, with Cretaceous sediments  
448 overstepping the fault with no offset (Fig. 5). The absence of Cretaceous sediments in the  
449 Central and Southern Slyne sub-basins obscures any fault activity that may have occurred  
450 during this period (Fig. 12B). Nevertheless, due to the pervasive nature of Cretaceous faulting  
451 in the Northern Slyne Sub-basin and strong evidence of Cretaceous faulting in the Porcupine  
452 Basin to the southwest (Jones & Underhill, 2011; Saqab et al., 2020), it is likely that some  
453 structures in the Central and Southern Slyne sub-basins were active during the Cretaceous.  
454 The motion on these faults would likely have been less than 100 ms TWTT in a similar manner  
455 to those in the Northern Slyne Sub-basin. Alongside the reactivation of Jurassic syn-rift faults,  
456 the majority of which were oriented NNE-SSW parallel to the axis of the Slyne Basin, a new



457 set of ENE-WSW oriented faults formed during the Cretaceous, observed offsetting the upper  
 458 100-200 ms TWTT of the Upper Jurassic section and the Cretaceous section in the Northern  
 459 Slyne Sub-basin (O'Sullivan & Childs, 2021).

Exhumation estimate (Km)	Location	Source
0.7-1.9	27/13-1	Scotchman & Thomas, 1995
0.8-1.7	Corrib	Corcoran & Mecklenburgh, 2005
0.7-3.2	Central and Southern Slyne sub-basins	Biancotto & Hardy, 2007
1.6-2.0	27/24-sb02	Fugro, 1994b
1.8	27/5-1	Geotrack, 1996
0.8-2.6	19/8-1	Geotrack, 2008

460 **Table 1:** Exhumation estimates from different locations throughout the Slyne Basin. Well  
 461 locations are shown in Figures 1 and 3.



462 **Figure 12: A)** TWTT thickness map (isochron) of the Cenozoic section in the Slyne and  
 463 southern Erris Basins superimposed on the main syn-rift structural features. A thicker Cenozoic  
 464 section is observed along the margin of the Rockall Basin on the western margin of the  
 465 Northern sub-basin and in the southern Erris Basin. This is transected by modern slope  
 466 canyons which incise into the Cenozoic section. A thicker Cenozoic section is also observed  
 467 in the Central sub-basin. **B)** TWTT thickness map (isochron) for the Cretaceous section in the  
 468 Slyne and southern Erris Basins superimposed on the main syn-rift structural features.  
 469 Cretaceous strata are absent in the Slyne Basin south of the Central Slyne Transfer Zone but  
 470 is present in the North Porcupine Basin. A significantly thicker Cretaceous section is preserved  
 471 in the southern Erris Basin, although it is eroded along the north-western margin of the Erris  
 472 Basin.  
 473



474 A second period of uplift and erosion occurred during the early Cenozoic throughout the Slyne  
475 Basin, forming another regional unconformity (Fig. 4-8). This was accompanied by a period of  
476 regional magmatism, expressed as igneous intrusions observed throughout the Slyne Basin  
477 (Fig. 4, 6, 7, 8) and layers of basaltic lava in the Northern and Southern Slyne sub-basins (Fig.  
478 4, 7).

479 Cenozoic tectonic activity reactivated several structures throughout the Slyne Basin with  
480 different expressions and senses of motion in different sub-basins; In the Northern Slyne Sub-  
481 basin the delamination fault above the Corrib anticline was reactivated for a second time,  
482 offsetting the early Eocene lavas of the Druid Formation, alongside the large listric fault to the  
483 west of Corrib (Fig. 7). In the Central and Southern Slyne sub-basins, several intra-basinal  
484 faults were reactivated, with both normal and reverse motion observed on faults with Cenozoic  
485 throw between 10 to 50 ms TWTT (Fig. 5). The large listric fault in the Central Slyne-Sub basin  
486 was inverted along with some of the rafted fault blocks along the eastern margin of the basin  
487 (Fig. 5). In the Central Slyne Sub-basin the bounding fault along the western margin of the  
488 basin was reactivated during the Cenozoic, with between 50-150 ms TWTT of throw recorded  
489 along its length (Fig. 5, 12A). The faults bounding the Northern Slyne Sub-basin were not  
490 reactivated during the Cenozoic (Fig. 6-8, 12A) but due to thermal subsidence in the  
491 neighbouring Rockall Basin the Cenozoic sequence thickens significantly along the western  
492 margin of the Northern Slyne Sub-basin (Fig. 7, 8, 12A).

## 493 7. Discussion

### 494 7.1. Structural inheritance and the impact of oblique pre- 495 existing structures

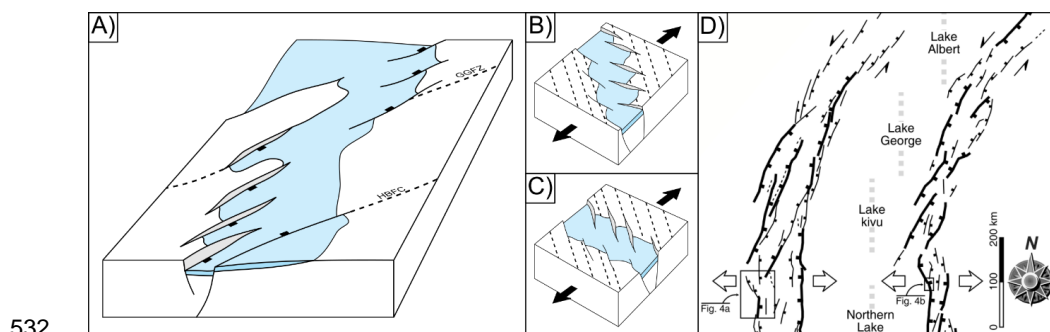
496 Structural inheritance is a common feature across the sedimentary basins of NW Europe, with  
497 Carboniferous, Permian, Jurassic and Cretaceous rifting interpreted to reactive older, pre-  
498 existing structures which formed during the Caledonian or Variscan Orogenies. This is  
499 recorded along the Atlantic margin of NW Europe (Stein, 1988; Doré et al., 1999; Ziegler &  
500 Dèzes, 2006; Schiffer et al., 2019) as well as in the basins of the North Sea (Fazlikhani et al.,  
501 2017; Philips et al., 2019; Osagiede et al., 2020). The reactivation of structures has been  
502 observed both onshore and offshore Ireland, with faults in the Carboniferous basins in the Irish  
503 midlands forming parallel to the NE-SW structures in the Caledonian basement (Worthington  
504 & Walsh, 2011; Kyne et al., 2019), while Variscan structures form the template for the later  
505 development of the Celtic Sea basins (Van Hoorn, 1987; Shannon, 1991; Rodriguez-Salgado  
506 et al., 2019). Similar relationships have been suggested for the Irish Atlantic margin (Tate &





507 Dobson, 1989; Naylor & Shannon, 2005), with several Caledonian structures mapped onshore  
 508 continuing into the offshore domain (Fig. 1).

509 The relationship between pre-existing basement structure and basin formation has been  
 510 studied extensively from outcrop and subsurface mapping and using analogue modelling (e.g.  
 511 Tommasi & Vauchez, 2001; Fazlikhani et al., 2017; Collanega et al., 2019). The key factor  
 512 that determines the nature of this relationship is the relative orientation of inherited structure  
 513 and the later extension direction (e.g. Henza et al., 2011; Henstra et al., 2015). Where  
 514 inherited structures are at a low angle to the extension direction, they are not reactivated but  
 515 may impede the propagation of new extensional faults and may give rise to transfer zones  
 516 between adjacent fault/basin segments. As the angle between pre-existing structures and  
 517 extension direction increases the likelihood of reactivation of basement structure increases  
 518 and analogue modelling has demonstrated the variety of fault patterns that can form in the  
 519 cover sequence. Although the effect of basement structure can be manifest in many ways the  
 520 two situations that have received most attention are extension oblique to an individual  
 521 basement fault (Schlishe et al., 2002) and oblique basin opening modelled by extension  
 522 oblique to a zone of weakness (Agostini et al., 2009; Philippon & Corti, 2016). In both cases  
 523 extension results in the formation of new fault segments, or faults, that are normal, or close to  
 524 normal, to the extension direction and arranged en echelon above or within the basement  
 525 structure or zone. Figure 13B illustrates fault/basin geometry that is characteristic of extension  
 526 oblique to a basement fabric; the key feature is that the overall orientation of the structure is  
 527 parallel to the basement structure. The Slyne Basin does not follow Caledonian basement  
 528 structure but cuts across it and as a result displays a different style of inheritance. Figure 13A  
 529 illustrates our interpretation of the initial Jurassic geometry of the Slyne Basin that is based on  
 530 observations below; this geometry resembles that in Fig. 13C in which individual fault  
 531 segments follow the basement trend but the basin as a whole cuts across it.



532

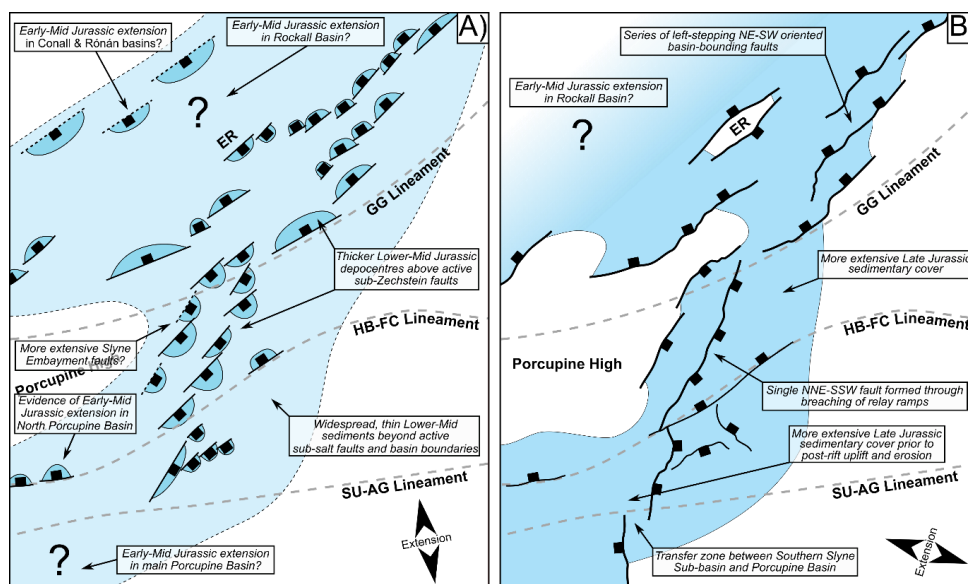
533 **Figure 13: A)** Schematic block model showing the initial fault segments of the basin bounding  
 534 faults and the reversal in basin polarity across the GGFZ. **B-C)** Block models showing  
 535 different patterns of basement formation when extension is oblique to pre-existing structures.



536 **D)** Section of Figure 3 of Corti et al. (2007) demonstrating similar rift geometries to those  
537 observed in the Slyne Basin.

538 The Slyne Basin strikes NNE-SSW ( $020^\circ$ ) and cuts across the local Caledonian inherited trend  
539 oriented NE-SW (c.  $045^\circ$ ). On the eastern flank of the Northern Slyne Sub-basin the bounding  
540 faults parallel the Caledonian trend and form a left stepping fault array (Fig. 1). The map  
541 pattern on the western flank is somewhat obscured by erosion and data quality but the faults  
542 also parallel the Caledonian trend. Within the Central Slyne Basin the faults offsetting the  
543 Jurassic are predominantly parallel to the basin axis (Fig. 11A). The majority of these faults  
544 are confined to the Jurassic section and are decoupled from the Carboniferous basement by  
545 the Zechstein salt (Fig. 5). The fault forming the western flank of the Central Slyne Basin is  
546 approximately parallel to the basin trend (Fig. 1) but closer inspection (Fig. 11A) shows that it  
547 has a distinct splay in the sub-salt basement. This fault pattern is consistent with this margin  
548 of the basin originating as a left-stepping fault array that would have comprised fault segments  
549 parallel to the preserved splays i.e. at a strike of ca.  $040^\circ$  and close to the orientation of the  
550 Caledonian basement fabric. We suggest therefore that the main faults that bound the Slyne  
551 Basin during Jurassic extension initially comprised left stepping arrays of fault segments that  
552 individually followed the Caledonian NE-SW trend (Fig. 13A, 14). This initial segmentation is  
553 preserved in the fault array bounding the eastern margin of the North Slyne Sub-basin but was  
554 bypassed by the formation of a through-going, basin-parallel (i.e. NNE-SSW oriented) fault in  
555 the Central Slyne Sub-basin. One of the main Caledonian structures that transects the basin,  
556 the Great Glen Fault Zone, was one of the structures reactivated to form a segment of the  
557 eastern margin of the North Slyne Basin and also perhaps one of the segments of the western  
558 margin of the Central Slyne Basin (the bounding fault of the Slyne Embayment), acted as the  
559 zone across which the basin reversed polarity.





560

561 **Figure 14:** Conceptual maps showing the evolution of the main basin-bounding and intra-  
 562 basinal faults in the Slyne Basin and surrounding areas during the **A)** Early to Middle Jurassic  
 563 and **B)** Late Jurassic.

564 The Slyne Basin provides an example of a form of basement control that is not frequently  
 565 documented in the literature. In general, individual faults are sub-perpendicular to the  
 566 extension direction, whether they be segments of a fault located above a reactivated basement  
 567 structure or faults within an oblique rift. The Slyne Basin cuts across the basement trend but  
 568 the individual basin bounding faults follow the basement trend. These two styles of interaction  
 569 are compared in Figure 13B and 13C. A key difference between these is that there is a reversal  
 570 of the sense of stepping of the basin bounding faults despite the fact that the angular  
 571 relationship between the basement and the extension direction is the same. This style of  
 572 inheritance is not generally recognised in analogue modelling, but Corti et al. (2007) generated  
 573 this pattern by introducing discrete narrow zones of weakness (Fig. 13D). Their model,  
 574 designed to replicate the structure of the western branch of the East African Rift System,  
 575 generated left-stepping rift-bounding faults in the presence of E-W extension by reactivation  
 576 of discrete crustal structures in a pattern very similar to that seen in the Slyne Basin. While  
 577 this style of inheritance is perhaps unusual, there are other areas in which it can be observed.  
 578 In the northern North Sea, a Triassic-Jurassic broadly N-S rift system formed on crust with  
 579 both N-S and NE-SW oriented Devonian and Caledonian crustal structures display a wide  
 580 variety of styles of inheritance (Fazilkhani et al. 2017; Phillips et al. 2019) but a common  
 581 feature is that major faults that parallel Caledonian trends are left stepping and the map pattern  
 582 of the Viking Graben, for example, is similar to that of the East African Rift shown in Fig.13D.



## 583 7.2. Post-rift uplift and erosion

584 A significant section of the syn-rift section is absent from the Slyne Basin, with key structural  
585 geometries recorded in the Upper Jurassic syn-rift sequences missing due to kilometre-scale  
586 uplift and erosion during the Cretaceous and Cenozoic (Table 1). The magnitude of uplift and  
587 erosion throughout the Slyne and Erris basins is highly variable. Previous authors have  
588 recorded a wide range of values for the magnitude of this post-rift exhumation, ranging from a  
589 few hundred metres to several kilometres (Scotchman & Thomas, 1995; Corcoran & Clayton,  
590 2001; Doré et al., 2002; Corcoran & Mecklenburgh, 2005; Biancotto et al., 2007). This  
591 variability in exhumation estimates arises due to the geological complexity associated with this  
592 process; in the Slyne Basin, three discrete post-rift unconformities are observed: the Base-  
593 Cretaceous, Base-Cenozoic and mid-Miocene unconformities. These unconformities are the  
594 result a variety of local and regional tectonic processes, including rift-shoulder uplift associated  
595 with rifting and hyperextension in the neighbouring Rockall Basin, the development of the  
596 Icelandic plume and the North Atlantic Igneous Province, ridge-push at the Mid-Atlantic Ridge,  
597 the Alpine Orogeny, and possibly the development of the Brendan Igneous Centre (Fig. 1, 2;  
598 Mohr, 1982). Additionally, these unconformities become composite surfaces at different  
599 locations within the Slyne basin: the absence of Cretaceous strata in the Central and Southern  
600 Slyne Sub-basins (Fig. 12B) may be due to non-deposition, or more likely, the erosion of the  
601 thin Cretaceous section, similar to that observed in the Northern Slyne Sub-basin, during the  
602 Cenozoic uplift events. The formation of these composite unconformities obscures the  
603 reactivation of any syn-rift faults in the Central and Southern Slyne Sub-basins during the  
604 Cretaceous, as the circa 100-300 m of erosion at the Base-Cenozoic Unconformity (sensu  
605 Corcoran & Mecklenburgh, 2005) is greater than the throw recorded on most of the  
606 Cretaceous faults observed in the Northern Slyne Sub-basin (Fig. 6, 7). Finally, the multitude  
607 of methodologies used to estimate exhumation varies throughout the basin, and includes  
608 vitrinite reflectance (Scotchman & Thomas, 1995; Corcoran & Clayton, 2001), compaction  
609 analysis (Corcoran & Mecklenburgh, 2005), and analysis of seismic velocities (Biancotto et  
610 al., 2007).

611 A further consequence of this extensive and variable erosion during the Cretaceous and  
612 Cenozoic is that the present-day boundaries of the basin are not representative of their full  
613 extent during the main syn-rift period. The Mesozoic rift basins on the Irish Atlantic margin,  
614 including the Slyne Basin, were much more extensive prior to uplift and erosion. Consequently,  
615 some publications have, as a result, focused on individual basins as separate and different  
616 geological entities rather than as residual parts of a complex, margin-wide rift system. Possible  
617 reconstructions of the Slyne Basin and neighbouring areas during the Early-Middle and Late  
618 Jurassic periods are presented in Figure 14.



### 619        7.3.    The Slyne Basin in the context of the Irish Atlantic 620            margin

621    As stated above, the Slyne Basin belongs to a framework of basins which stretch across the  
622    Irish Atlantic margin and likely shares aspects of its geological evolution with these other  
623    areas. The most similar of these neighbours is the Erris Basin directly north of the Northern  
624    Slyne Sub-basin (Fig. 1). The Erris Basin is contiguous with and has a similar sedimentary fill  
625    to the Slyne Basin which suggest that both basins underwent a similar geological evolution  
626    during the Permian, Triassic and Jurassic periods (Fig. 8). The evolution of the Slyne and Erris  
627    basins diverges in the Cretaceous, with the thicker Cretaceous section in the Erris Basin (Fig.  
628    8, 12B) indicating it underwent active extension during the Cretaceous alongside the  
629    neighbouring Rockall Basin while the Slyne Basin remained largely inactive.

630    The Slyne Basin is separated from the Porcupine Basin by a narrow basement high  
631    approximately five kilometres wide (Fig. 4). This high is the eroded footwall of the fault  
632    bounding the Southern Slyne Sub-basin, with kilometre-scale erosion largely taking place  
633    during the Cretaceous and Cenozoic (Dancer et al., 1999; Biancotto et al, 2007). Restoring a  
634    kilometre-scale section of Upper Jurassic stratigraphy would connect the Porcupine Basin with  
635    the Southern Slyne Sub-basin, supporting the idea that these basins developed coevally  
636    during the Late Jurassic (Fig. 14B). The nearby 26/30-1 well in the Porcupine Basin (Fig. 4)  
637    encountered the Upper Jurassic Minard Formation resting unconformably atop the  
638    Carboniferous Blackthorn Group (Phillips Petroleum Company, 1982), while the intervening  
639    Permian to Middle Jurassic stratigraphy present in the Southern Slyne Sub-basin is absent.  
640    While Triassic and Lower Jurassic stratigraphy has been encountered in two wells in the North  
641    Porcupine Basin to the north of the Finnian's Spur (Fig. 1B; Bulois et al., 2018; Merlin Energy  
642    Resources Consortium, 2020), most wells in the Northern Porcupine Basin encountered  
643    Upper Jurassic sediments resting directly atop Carboniferous sediments (Merlin Energy  
644    Resources Consortium, 2020). Permian sediments have not been encountered in any well in  
645    the Porcupine Basin (Merlin Energy Resources Consortium, 2020). This indicates that the  
646    Slyne Basin is the older of the two basins, with extension beginning in the Late Permian with  
647    the deposition of several 100 metres of Zechstein Group evaporites (Štolfová & Shannon,  
648    2009; O'Sullivan et al., 2021) while the Northern Porcupine likely remained a relative high  
649    during the latest Palaeozoic and early Mesozoic. There may be narrow outliers of Permian,  
650    Triassic and Early to Middle Jurassic-aged sediments preserved beneath the Late Jurassic  
651    sediments further south in the Porcupine Basin, but at present this remains unproven.



## 652 8. Conclusions

653 Detailed interpretation of available seismic reflection data in conjunction with borehole and  
654 potential-field datasets has delivered an improved understanding of the complex and  
655 multiphase structural history of the Slyne Basin.

- 656 1. The onset of rifting in the Slyne Basin began in the Late Permian, expressed as diffuse  
657 extensional faulting accompanied by the deposition of the Zechstein Group evaporites in  
658 localised, fault-bounded depocentres. This was followed by tectonic quiescence during the  
659 majority of the Triassic and subsequent extension accompanied by localised halokinesis  
660 during the Latest Triassic and into the Early and Middle Jurassic. Regional uplift and  
661 erosion occurred during the late Middle Jurassic, creating a regional unconformity. The  
662 main phase of rifting began in the Oxfordian and continued until the end of the Jurassic.
- 663 2. The Slyne Basin experienced kilometre-scale uplift and erosion throughout the Early  
664 Cretaceous, creating the distinct angular unconformity between Jurassic syn-rift  
665 sediments and Cretaceous and younger post-rift sediments. Subsequent and less-severe  
666 phases of exhumation occurred during the Cenozoic. Faults throughout the basin are  
667 reactivated in both normal and reverse senses during this tectonic activity.
- 668 3. The segmentation of the Slyne Basin into discrete sub-basins occurs where crustal-scale  
669 structural lineaments, representing the suture zones and boundaries between Caledonian  
670 and Precambrian terranes, obliquely transect the younger Mesozoic basin.
- 671 4. The basin axis is oriented NNE-SSW and cuts across the N-E Caledonian trend resulting  
672 in a rarely documented style of fault reactivation in which the segments of basin-bounding  
673 faults follow the earlier structural grain but the basin as a whole does not. As strain  
674 increased initial left-stepping segments linked resulting in basin-bounding faults oriented  
675 parallel to the basin axis.
- 676 5. Salt layers in the Slyne Basin exert important controls on basin-development, most  
677 importantly acting as décollements between the Palaeozoic pre-salt basement and  
678 Mesozoic post-salt basin-fill. The most important salt-prone interval is the Permian  
679 Zechstein Group, present throughout the Slyne Basin, while in the Northern sub-basin the  
680 Upper Triassic Uilleann Halite Member is also present, acting as a second layer of  
681 mechanical detachment.

## 682 9. Data availability

683 The data that support the findings of this study were provided by the Petroleum Affairs Division  
684 (PAD) and are available for download from [https://www.dccae.gov.ie/en-ie/natural-](https://www.dccae.gov.ie/en-ie/natural-resources/topics/Oil-Gas-Exploration-Production/data/Pages/Data.aspx)  
685 [resources/topics/Oil-Gas-Exploration-Production/data/Pages/Data.aspx](https://www.dccae.gov.ie/en-ie/natural-resources/topics/Oil-Gas-Exploration-Production/data/Pages/Data.aspx). Restrictions may  
686 apply to the availability of these data, which were used under licence for this study.





687 **10. Author contribution**

688 Conor O'Sullivan carried out data analysis, wrote the original text, drafted the figures, and  
689 conceptualised the original ideas presented therein. Conrad Childs and Mudasar Saqab  
690 provided initial project conceptualisation, supervision and reviewed the final text. John Walsh  
691 and Patrick Shannon reviewed the final text.

692 **11. Declaration of competing interests**

693 The authors declare that they have no known competing financial interests or personal  
694 relationships that could have appeared to influence the work reported in this paper.

695 **12. Acknowledgements**

696 This research is funded in part by a research grant from Science Foundation Ireland (SFI)  
697 under Grant Number 13/RC/2092 and is co-funded under the European Regional  
698 Development Fund, and by the Petroleum Infrastructure Programme (PIP) and its member  
699 companies. Efstratios Delogkos is thanked for thoughtful discussions regarding the links  
700 between the Slyne Basin and the Bróna and Pádraig basins. Karize Oudit, Neil Jones, Blanca  
701 Cantalejo Lopez and Andrew King of CNOOC International are thanked for engaging  
702 discussions on the structural evolution of the Slyne Basin. Phil Copestake of Merlin Energy  
703 Resources Limited is thanked for providing additional detail on revised biostratigraphic  
704 interpretation of the Slyne Basin. The authors would like to thank the Petroleum Affairs Division  
705 (PAD) of the Department of Communications, Climate Action and Environment (DCCAE),  
706 Ireland, for providing access to released well, seismic and potential field datasets. Europa Oil  
707 & Gas are thanked for providing access to the Inishkea 2018 reprocessed 3D volume and  
708 allowing an arbitrary line from the volume to be shown. Shell Exploration & Production Ireland  
709 Ltd. are thanked for providing access to reprocessed volumes of the 1997 Corrib 3D. The  
710 authors would also like to thank Schlumberger for providing academic licenses of Petrel to  
711 University College Dublin.

712



713 13. References

- 714 Ady, B.E. & Whittaker, R.C.: Examining the influence of tectonic inheritance on the evolution  
715 of the North Atlantic using a palinspastic deformable plate reconstruction. *Geological*  
716 *Society, London, Special Publications*, **470**, 245–264, <https://doi.org/10.1144/SP470.9>.  
717 2019.
- 718 Agostini, A., Corti, G., Zeoli, A. & Mulugeta, G.: Evolution, pattern, and partitioning of  
719 deformation during oblique continental rifting: Inferences from lithospheric-scale  
720 centrifuge models. *Geochemistry, Geophysics, Geosystems*, *10*(11). 2009.
- 721 Alves, T.M., Moita, C., Sandnes, F., Cunha, T., Monteiro, J.H. & Pinheiro, L.M.: Mesozoic-  
722 Cenozoic evolution of North Atlantic continental-slope basins: The Peniche basin,  
723 western Iberian margin. *AAPG Bulletin*, **90**, 31–60,  
724 <https://doi.org/10.1306/08110504138>. 2006.
- 725 Anderson, H., Walsh, J.J. & Cooper, M.R.: The development of a regional-scale intraplate  
726 strike-slip fault system; Alpine deformation in the north of Ireland. *Journal of Structural*  
727 *Geology*, **116**, 47–63. 2018.
- 728 Badley, M.E.: Late Tertiary faulting, footwall uplift and topography in western Ireland.  
729 *Geological Society, London, Special Publications*, **188**, 201–207,  
730 <https://doi.org/10.1144/GSL.SP.2001.188.01.11>. 2001.
- 731 Biancotto, F., Hardy, R.J.J., Jones, S.M., Brennan, D. & White, N.J.: Estimating denudation  
732 from seismic velocities offshore northwest Ireland. In: *SEG Technical Program*  
733 *Expanded Abstracts 2007*. Society of Exploration Geophysicists, 407–411. 2007.
- 734 Bird, P.C., Cartwright, J.A. & Davies, T.L.: Basement reactivation in the development of rift  
735 basins: an example of reactivated Caledonide structures in the West Orkney Basin.  
736 *Journal of the Geological Society*, **172**, 77–85. 2014.
- 737 Brown, A.R.: Calibrate yourself to your data! A vital first step in seismic interpretation.  
738 *Geophysical Prospecting*, **49**, 729–733. 2001.
- 739 Bulois, C., Pubellier, M., Chamot-Rooke, N. & Watremez, L.: From orogenic collapse to  
740 rifting: A case study of the northern Porcupine Basin, offshore Ireland. *Journal of*  
741 *Structural Geology*, **114**, 139–162, <https://doi.org/10.1016/j.jsg.2018.06.021>. 2018.
- 742 Chapman, T.J., Broks, T.M., Corcoran, D.V., Duncan, L.A. & Dancer, P.N.: The structural  
743 evolution of the Erris Trough, offshore northwest Ireland, and implications for  
744 hydrocarbon generation. *Petroleum Geology of Northwest Europe: Proceedings of the*  
745 *5th Conference*, 455–469. 1999.
- 746 Collanega, L., Siuda, K., Jackson, C. A.-L., Bell, R.E., Coleman, A.J., Lenhart, A., Magee, C.  
747 & Breda, A.: Normal fault growth influenced by basement fabrics: The importance of  
748 preferential nucleation from pre-existing structures. *Basin Research*, **31**, 659–687,  
749 <https://doi.org/10.1111/bre.12327>. 2019.
- 750 Corcoran, D. V & Doré, A.G.: Depressurization of hydrocarbon-bearing reservoirs in  
751 exhumed basin settings: evidence from Atlantic margin and borderland basins.



- 752 *Geological Society, London, Special Publications*, **196**, 457–483,  
753 <https://doi.org/10.1144/GSL.SP.2002.196.01.25>. 2002.
- 754 Corcoran, D. V & Mecklenburgh, R.: Exhumation of the Corrib Gas Field, Slyne Basin,  
755 offshore Ireland. *Petroleum Geoscience*, **11**, 239–256. 2005.
- 756 Corfield, S., Murphy, N. & Parker, S.: The structural and stratigraphic framework of the Irish  
757 Rockall Trough. *Petroleum Geology Conference Proceedings*, **5**, 407–420,  
758 <https://doi.org/10.1144/0050407>. 1999.
- 759 Corti, G., van Wijk, J., Cloetingh, S. & Morley, C.K.: Tectonic inheritance and continental rift  
760 architecture: Numerical and analogue models of the East African Rift system.  
761 *Tectonics*, **26**, n/a-n/a, <https://doi.org/10.1029/2006TC002086>. 2007.
- 762 Cunningham, G.A. & Shannon, P.M.: The Erris Ridge: A major geological feature in the NW  
763 Irish Offshore Basins. *Journal of the Geological Society*, **154**, 503–508. 1997.
- 764 Dancer, P.N., Algar, S.T. & Wilson, I.R.: Structural evolution of the Slyne Trough. *Petroleum  
765 Geology of Northwest Europe: Proceedings of the 5th Conference on the Petroleum  
766 Geology of Northwest Europe*, **1**, 445–454. 1999.
- 767 Dancer, P.N. & Pillar, N.W.: Exploring in the Slyne Basin: a geophysical challenge. *The  
768 Petroleum Exploration of Ireland's Offshore Basins*, **188**, 209–222. 2001.
- 769 Dancer, P.N., Kenyon-Roberts, S.M., Downey, J.W., Baillie, J.M., Meadows, N.S. & Maguire,  
770 K.: The Corrib gas field, offshore west of Ireland. *Geological Society, London,  
771 Petroleum Geology Conference series*, **6**, 1035–1046. 2005.
- 772 Doré, A.G., Lundin, E.R., Jensen, L.N., Birkeland, O., Eliassen, P.E. & Fichler, C.: Principal  
773 tectonic events in the evolution of the northwest European Atlantic margin. *Petroleum  
774 Geology of Northwest Europe: Proceedings of the 5th Conference*, 41–61. 1999.
- 775 Doré, A.G., Lundin, E.R., Fichler, C. & Olesen, O.: Patterns of basement structure and  
776 reactivation along the NE Atlantic margin. *Journal of the Geological Society*, **154**, 85–9.  
777 2007.
- 778 Droujinine, A., Buckner, S. & Cameron, R.: Full-wave long offset seismic imaging and  
779 velocity analysis with gravity and well constraints — a case study from NW Corrib,  
780 offshore Ireland. In: *SEG Technical Program Expanded Abstracts 2005*. Society of  
781 Exploration Geophysicists, 409–412. 2005.
- 782 Duffy, O.B., Gawthorpe, R.L., Docherty, M. & Brocklehurst, S.H.: Mobile evaporite controls  
783 on the structural style and evolution of rift basins: Danish Central Graben, North Sea.  
784 *Basin Research*, **25**, 310–330, <https://doi.org/10.1111/bre.12000>. 2013.
- 785 Fazlikhani, H., Fossen, H., Gawthorpe, R.L., Faleide, J.I. & Bell, R.E.: Basement structure  
786 and its influence on the structural configuration of the northern North Sea rift. *Tectonics*,  
787 **36**, 1151–1177, <https://doi.org/10.1002/2017TC004514>. 2017.
- 788 Fugro.: Field Report Irish Frontier Shallow Coring Project Blocks 19/13 and 27/24 Irish  
789 Sector Atlantic Ocean (Volume I). 1994a.



- 790 Fugro.: Field Report Irish Frontier Shallow Coring Project Blocks 19/13 and 27/24 Irish  
791 Sector Atlantic Ocean (Volume II). 1994b.
- 792 Gawthorpe, R.L. & Hurst, J.M.: Transfer zones in extensional basins: their structural style  
793 and influence on drainage development and stratigraphy. *Journal of the Geological*  
794 *Society*, **150**, 1137–1152. 1993.
- 795 Geotrack.: Thermal history reconstruction in well 27/5-1 west of Ireland using apatite fission  
796 track analysis and vitrinite reflectance. Report compiled by Gibson, H.J. 1996.
- 797 Geotrack.: Thermal history reconstruction in offshore Ireland well 19/8-1, based on AFTA®  
798 and VR data. Report compiled by Green, P.F. 2008.
- 799 Hardy, R.J.J., Querendez, E., Biancotto, F., Jones, S.M., O’Sullivan, J. & White, N.: New  
800 methods of improving seismic data to aid understanding of passive margin evolution: a  
801 series of case histories from offshore west of Ireland. *Petroleum Geology: From Mature*  
802 *Basins to New Frontiers—Proceedings of the 7th Petroleum Geology Conference*, **7**,  
803 1005–1012. 2010.
- 804 Henstra, G.A., Rotevatn, A., Gawthorpe, R.L. & Ravnås, R.: Evolution of a major segmented  
805 normal fault during multiphase rifting: The origin of plan-view zigzag geometry. *Journal*  
806 *of Structural Geology*, **74**, pp.45-63. 2015.
- 807 Henza, A.A., Withjack, M.O. & Schlische, R.W.: How do the properties of a pre-existing  
808 normal-fault population influence fault development during a subsequent phase of  
809 extension?. *Journal of Structural Geology*, **33**(9), pp.1312-1324. 2011.
- 810 Hudec, M.R. & Jackson, M.P.A.: Terra infirma: Understanding salt tectonics. *Earth-Science*  
811 *Reviews*, **82**, 1–28, <https://doi.org/10.1016/j.earscirev.2007.01.001>. 2007.
- 812 Jackson, C.A.L. & Lewis, M.M.: Structural style and evolution of a salt-influenced rift basin  
813 margin; the impact of variations in salt composition and the role of polyphase extension.  
814 *Basin Research*, **28**, 81–102, <https://doi.org/10.1111/bre.12099>. 2016.
- 815 Jackson, C.A.L., Elliott, G.M., Royce-Rogers, E., Gawthorpe, R.L. & Aas, T.E.: Salt  
816 thickness and composition influence rift structural style, northern North Sea, offshore  
817 Norway. *Basin Research*, **31**, 514–538, <https://doi.org/10.1111/bre.12332>. 2019.
- 818 Kimbell, G.S., Ritchie, J.D. & Henderson, A.F.: Three-dimensional gravity and magnetic  
819 modelling of the Irish sector of the NE Atlantic margin. *Tectonophysics*, **486**, 36–54,  
820 <https://doi.org/10.1016/j.tecto.2010.02.007>. 2010.
- 821 Kyne, R., Torremans, K., Güven, J., Doyle, R. & Walsh, J.: 3-D modeling of the Lisheen and  
822 silvermines deposits, County Tipperary, Ireland: insights into structural controls on the  
823 formation of Irish Zn-Pb deposits. *Economic Geology*, **114**, 93–116,  
824 <https://doi.org/10.5382/econgeo.2019.4621>. 2019.
- 825 Lefort, J.P. & Max, M.D.: Development of the Porcupine Seabight: use of magnetic data to  
826 show the direct relationship between early oceanic and continental structures. *Journal*  
827 *of the Geological Society*, **141**, 663–674, <https://doi.org/10.1144/gsjgs.141.4.0663>.  
828 1984.





- 829 McKie, T. & Shannon, P.M.: Comment on ‘The Permian-Triassic transition and the onset of  
830 Mesozoic sedimentation at the northwestern peri Tethyan domain scale:  
831 Palaeogeographic maps and geodynamic implications’ by S. Bourquin, A. Bercovici, J.  
832 López-Gomez, J. B. Diez, J. Broutin, A. . *Palaeogeography, Palaeoclimatology,  
833 Palaeoecology*, **311**, 136–143, <https://doi.org/10.1016/j.palaeo.2011.07.016>. 2011.
- 834 Merlin Energy Resources Consortium: The Standard Stratigraphic Nomenclature of Offshore  
835 Ireland: An Integrated Lithostratigraphic, Biostratigraphic and Sequence Stratigraphic  
836 Framework. Project Atlas. Petroleum Affairs Division, Department of the Environment,  
837 Climate and Communications, Special Publication **1/21**. 2020.
- 838 Mohr, P.: Tertiary dolerite intrusions of west-central Ireland. *Proceedings, Royal Irish  
839 Academy*, **82B**, 53–82. 1982.
- 840 Morley, C.K., Nelson, R. a, Patton, T.L. & Munn, S.G.: Transfer Zones in the East African  
841 Rift System and Their Relavance to Hydrocarbon Exploration in Rifts. *American  
842 Association of Petroleum Geologists Bulletin*, **74**, No. 8, 1234–1253. 1990.
- 843 Morley, C.K., Haranya, C., Phoosongsee, W., Pongwapee, S., Kornawan, A. & Wonganan,  
844 N.: Activation of rift oblique and rift parallel pre-existing fabrics during extension and  
845 their effect on deformation style: examples from the rifts of Thailand. *Journal of  
846 Structural Geology*, **26**, 1803–1829. 2004.
- 847 Musgrove, F.W. & Mitchener, B.: Analysis of the pre-tertiary rifting history of the Rockall  
848 Trough. *Petroleum Geoscience*, **2**, 353–360, <https://doi.org/10.1144/petgeo.2.4.353>.  
849 1996.
- 850 Naylor, D., Shannon, P. & Murphy, N.: *Irish Rockall Basin Region - a standard structural  
851 nomenclature system*. Petroleum Affairs Division, Special Publication 1/99. 1999.
- 852 Naylor, D. & Shannon, P.M.: The structural framework of the Irish Atlantic Margin. *Geological  
853 Society, London, Petroleum Geology Conference series*, **6**, 1009–1021,  
854 <https://doi.org/10.1144/0061009>. 2005.
- 855 O’Sullivan, C. & Childs, C.: Kinematic interaction between stratigraphically discrete salt  
856 layers; the structural evolution of the Corrib gas field, offshore NW Ireland. *Marine and  
857 Petroleum Geology*, **133**, 105274, <https://doi.org/10.1016/j.marpetgeo.2021.105274>.  
858 2021.
- 859 O’Sullivan, C.M., Childs, C.J., Saqab, M.M., Walsh, J.J. & Shannon, P.M.: The influence of  
860 multiple salt layers on rift-basin development; The Slyne and Erris basins, offshore NW  
861 Ireland. *Basin Research*, 1–31, <https://doi.org/10.1111/bre.12546>. 2021.
- 862 Osagiede, E.E., Rotevatn, A., Gawthorpe, R., Kristensen, T.B., Jackson, C.A.L. & Marsh, N.:  
863 Pre-existing intra-basement shear zones influence growth and geometry of non-colinear  
864 normal faults, western Utsira High–Heimdal Terrace, North Sea. *Journal of Structural  
865 Geology*, **130**, 103908, <https://doi.org/10.1016/j.jsg.2019.103908>. 2020.
- 866 Pereira, R. & Alves, T.M.: Margin segmentation prior to continental break-up: A seismic-  
867 stratigraphic record of multiphased rifting in the North Atlantic (Southwest Iberia).  
868 *Tectonophysics*, **505**, 17–34, <https://doi.org/10.1016/j.tecto.2011.03.011>. 2011.



- 869 Pereira, R., Alves, T.M. & Mata, J.: Alternating crustal architecture in West Iberia: A review  
870 of its significance in the context of NE Atlantic rifting. *Journal of the Geological Society*,  
871 **174**, 522–540, <https://doi.org/10.1144/jgs2016-050>. 2017.
- 872 Philippon, M. & Corti, G.: Obliquity along plate boundaries. *Tectonophysics*, **693**, pp.171-  
873 182. 2016.
- 874 Phillips Petroleum Company: Phillips Petroleum Company Ireland 26/30-1 Final Well Report.  
875 1982.
- 876 Phillips, T.B., Jackson, C.A., Bell, R.E. & Duffy, O.B.: Oblique reactivation of lithosphere-  
877 scale lineaments controls rift physiography – the upper-crustal expression of the  
878 Sorgenfrei–Tornquist Zone, offshore southern Norway. *Solid Earth*, **9**, 403–429. 2018.
- 879 Phillips, T.B., Fazlikhani, H., Gawthorpe, R.L., Fossen, H., Jackson, C.A.L., Bell, R.E.,  
880 Faleide, J.I. & Rotevatn, A.: The Influence of Structural Inheritance and Multiphase  
881 Extension on Rift Development, the Northern North Sea. *Tectonics*, **38**, 4099–4126,  
882 <https://doi.org/10.1029/2019TC005756>. 2019.
- 883 Robeson, D., Burnett, R.D. & Clayton, G.: The Upper Palaeozoic Geology of the Porcupine,  
884 Erris and Donegal Basins, Offshore Ireland. *Irish Journal of Earth Sciences*, **9**, 153–  
885 175. 1988.
- 886 Rodríguez-Salgado, P., Childs, C., Shannon, P.M. & Walsh, J.J.: Structural evolution and the  
887 partitioning of deformation during basin growth and inversion: A case study from the  
888 Mizen Basin Celtic Sea, offshore Ireland. *Basin Research*, 1–24,  
889 <https://doi.org/10.1111/bre.12402>. 2019.
- 890 Rohrman, M.: Prospectivity of volcanic basins: Trap delineation and acreage de-risking.  
891 *AAPG Bulletin*, **91**, 915–939. 2007.
- 892 Saqab, M.M., Childs, C., Walsh, J. & Delogkos, E.: Multiphase deformation history of the  
893 Porcupine Basin, offshore west Ireland. *Basin Research*, 1–22,  
894 <https://doi.org/10.1111/bre.12535>. 2020.
- 895 Schiffer, C., Doré, A.G., Foulger, G.R., Franke, D., Geoffroy, L., Gernigon, L., Holdsworth,  
896 R.E., Kuszniir, N., Lundin, E., McCaffrey, K., Peace, A.L., Petersen, K.D., Phillips, T.B.,  
897 Stephenson, R., Stoker, M.S. & Welford J.K.: Structural inheritance in the North  
898 Atlantic. *Earth-Science Reviews*, 102975.  
899 <https://doi.org/10.1016/j.earscirev.2019.102975>. 2019.
- 900 Schlische, R.W., Withjack, M.O. & Eisenstadt, G.: An experimental study of the secondary  
901 deformation produced by oblique-slip normal faulting. *AAPG bulletin*, **86**(5), pp.885-906.  
902 2002.
- 903 Schumacher, M.E.: Upper Rhine Graben: Role of preexisting structures during rift evolution.  
904 *Tectonics*, **21**. 2002.
- 905 Scotchman, I.C. & Thomas, J.R.W.: Maturity and hydrocarbon generation in the Slyne  
906 Trough, northwest Ireland. *The Petroleum Geology of Ireland's Offshore Basins*, **93**,  
907 385–412. 1995.



- 908 Shannon, P.M.: The development of Irish offshore sedimentary basins. *Journal of the*  
909 *Geological Society*, **148**, 181–189. 1991.
- 910 Shannon, P.M.: Old challenges, new developments and new plays in Irish offshore  
911 exploration. *Geological Society, London, Petroleum Geology Conference series*, **8**,  
912 171–185, <https://doi.org/10.1144/PGC8.12>. 2018.
- 913 Stein, A.M.: Basement controls upon basin development in the Caledonian foreland, NW  
914 Scotland. *Basin Research*, **1**, 107–119, <https://doi.org/10.1111/j.1365-2117.1988.tb00008.x>. 1988.
- 916 Štolfová, K. & Shannon, P.M.: Permo-Triassic development from Ireland to Norway: basin  
917 architecture and regional controls. *Geological Journal*, **44**, 652–676. 2009.
- 918 Tate, M.P.: The Clare Lineament: A relic transform fault west of Ireland. *Geological Society*  
919 *Special Publication*, **62**, 375–384, <https://doi.org/10.1144/GSL.SP.1992.062.01.28>.  
920 1992.
- 921 Tate, M.P. & Dobson, M.R.: Late Permian to early Mesozoic rifting and sedimentation  
922 offshore NW Ireland. *Marine and Petroleum Geology*, **6**, 49–59,  
923 [https://doi.org/10.1016/0264-8172\(89\)90075-5](https://doi.org/10.1016/0264-8172(89)90075-5). 1989.
- 924 Tommasi, A. & Vauchez, A.: Continental rifting parallel to ancient collisional belts: An effect  
925 of the mechanical anisotropy of the lithospheric mantle. *Earth and Planetary Science*  
926 *Letters*, **185**, 199–210, [https://doi.org/10.1016/S0012-821X\(00\)00350-2](https://doi.org/10.1016/S0012-821X(00)00350-2). 2001.
- 927 Trueblood, S. & Morton, N.: Comparative Sequence Stratigraphy and Structural Styles of the  
928 Slyne Trough and Hebrides Basin. *Journal of the Geological Society*, **148**, 197–201.  
929 1991.
- 930 Underhill, J.R. & Partington, M.A.: Jurassic thermal doming and deflation in the North Sea:  
931 Implications of the sequence stratigraphic evidence. *Petroleum Geology Conference*  
932 *Proceedings*, **4**, 337–345, <https://doi.org/10.1144/0040337>. 1993.
- 933 Van Hoorn, B.: The south Celtic Sea/Bristol Channel Basin: origin, deformation and inversion  
934 history. *Tectonophysics*, **137**, [https://doi.org/10.1016/0040-1951\(87\)90325-8](https://doi.org/10.1016/0040-1951(87)90325-8). 1987.
- 935 Vendeville, B.C. & Jackson, M.P.A.: The fall of diapirs during thin-skinned extension. *Marine*  
936 *and Petroleum Geology*, **9**, 354–371, [https://doi.org/10.1016/0264-8172\(92\)90048-J](https://doi.org/10.1016/0264-8172(92)90048-J).  
937 1992.
- 938 Walsh, A., Knag, G., Morris, M., Quinquis, H., Tricker, P., Bird, C. & Bower, S.: Petroleum  
939 geology of the Irish Rockall Trough – a frontier challenge. *Petroleum Geology of*  
940 *Northwest Europe: Proceedings of the 5th Conference*, 433–444. 1999.
- 941 Walsh, J.J. & Watterson, J.: Geometric and kinematic coherence and scale effects in normal  
942 fault systems. *Geological Society Special Publication*, **56**, 193–203,  
943 <https://doi.org/10.1144/GSL.SP.1991.056.01.13>. 1991.
- 944 Wilson, R.W., Holdsworth, R.E., Wild, L.E., McCaffrey, K.J.W., England, R.W., Imber, J. &  
945 Strachan, R.A.: Basement-influenced rifting and basin development: A reappraisal of  
946 post-Caledonian faulting patterns from the North Coast Transfer Zone, Scotland.



- 947            *Geological Society Special Publication*, **335**, 795–826,  
948            <https://doi.org/10.1144/SP335.32>. 2010.
- 949    Worthington, R.P. & Walsh, J.J.: Structure of Lower Carboniferous basins of NW Ireland,  
950            and its implications for structural inheritance and Cenozoic faulting. *Journal of*  
951            *Structural Geology*, **33**, 1285–1299. 2011.
- 952    Ziegler, P.A. & Dèzes, P.: Crustal evolution of Western and Central Europe. *Geological*  
953            *Society, London, Memoirs*, **32**, 43–56. 2006.